NTNU – Trondheim
Norwegian University of
Science and Technology

Master thesis in Marine Cybernetics

Spring 2012

Modelling and control of underwater inspection vehicle for aquaculture sites

Author:
Mats Nåvik Hval

Advisors:
Karl Gunnar Aarsæther
Per Rundtop

Supervisor:
Professor Asgeir J. Sørensen

Abstract

Underwater vehicles such as AUVs and ROVs with hovering capabilities is a promising method for inspection of net integrity in large scale, sea based, salmon farms. The location of the salmon farms cause underwater vehicles to be affected by strong tidal currents and waves. In this thesis a six degree of freedom unified process plant model combining seakeeping theory and maneuvering theory for a small work ROV called Argus Mariner is developed. Using the software WAMIT, the hydrodynamic potential coefficients and wave induced forces and moments are found. A basic control system for traversing a dynamic netcage model is developed. The models and control system are implemented in a simulation environment called FhSim developed by SINTEF Fishery and Aquaculture AS.

NTNU Trondheim
Norwegian University of Science and Technology
Department of Marine Technology

MASTER THESIS IN MARINE CYBERNETICS

SPRING 2012

STUD. TECHN. MATS NÅVIK HVAL

Modelling and control of underwater inspection vehicle for aquaculture sites

Work description:
The size of aquaculture sites are increasing and net cage with an area of 5000-8000m2 is not uncommon. With the net structure as the only barrier between the farmed fish and the ocean, inspection of the cages have to be carried out regularly. Today inspection and cleaning operations are carried out manually either by diver or ROV with a camera. If damages to the net are found, divers are put into the water to repair. These are time-consuming and expensive operations. Because the current technology has not been developed and specialized for typical aquaculture operations, development of automatic control algorithms for these operations can make fish farming more cost efficient and increase the safety, because more regularly inspection of the net will decrease the chance of fish escaping. The need for divers to repair damages will also decrease. The challenge is the dynamics of the system. Varying current and waves will cause the net cage structure to change shape and influence the motion of the ROV. To study the feasibility of automatic inspection, cleaning and repair a process plant model of an ROV will be made. Control algorithms for traversing a cage with varying shape will also be developed and tested in a simulator.

Scope of work:
1. Model Argus Remote System medium size work ROV, including rigid body dynamics, hydrodynamic forces and actuators.
2. Determine the parameters and coefficients for the ROV by using hydrodynamic software code and experience from ROV Minerva owned by NTNU.
3. Implement model in simulator software FhSim developed by SINTEF Fisheries and Aquaculture and combine with already existing models for net cage and environment.
4. Develop a 6DOF ROV-observer, controller and thrust allocation. Assume known global attitude and position measurements. Use fish cage model to get an estimate of the position and attitude of the net.
5. Develop reference generator for automatic traversing of fish cage and implement it in FhSim.
6. Perform simulations in FhSim to show ROV behaviour and performance.

Advisor: Per Rundtorp, SFH Advisor: Karl Gunnar Aarsæther, SFH

Professor Asgeir Sørensen
Supervisor

Acknowledgements

I would like to thank Thor I. Fossen for the discussion and great inputs on software for hydrodynamics. Per Rundtop and Karl Gunnar Aarsæther at SINTEF Fishery and Aquaculture for the introducing me to and helping me with the simulator used.

During the work with this thesis, the help and enthusiastic guidance of my supervisor professor Asgeir J. Sørensen has been greatly appreciated. His good mood and pleasant manner has helped me a lot during periods of great frustration. By sharing his knowledge in the most unusual ways he has given me great motivation and an urge of knowledge within the field of modelling and control engineering.

I would also use the opportunity to thank my fellow students at spesialization of marine cybernetics for their ability to always be available for questions and discussions, and especially Espen Tolpinrud for his constructive contributions and encouraging comments.

Mats Nåvik Hval
Trondheim, June 10. 2012

Contents

List of Figures

Nomenclature

$\boldsymbol{\nu}_{b/n}^{b}$	Body-fixed linear velocities
$\boldsymbol{\omega}_{b/n}^{b}$	Body-fixed angular velocities
$\boldsymbol{\tau}$	Forces and moments in body frame
$\boldsymbol{\Theta}_{bn}$	Attitude in the NED frame.
$\boldsymbol{\Delta}$	Reference damping matrix
$\boldsymbol{\eta}_{d}$	Desired position and attitude
$\boldsymbol{\eta}_{w}$	Contribution from wave model to vehicle position
$\hat{\boldsymbol{\eta}}$	position and attitude estimate vector
$\hat{\boldsymbol{\xi}}$	wave state vector
$\boldsymbol{\mu}$	Fluid memory effect
$\boldsymbol{\nu}_{c}$	Current velocity in body frame
$\boldsymbol{\nu}_{c}^{n}$	Current velocity in the NED frame
$\boldsymbol{\nu}_{r}$	Vehicle relative velocity
$\boldsymbol{\Omega}$	Reference rate of change tuning matrix
$\boldsymbol{\tau}^{XYZ}$	Thrust from one thruster in vehicle body frame
$\boldsymbol{\tau}_{c}$	Commanded thrust vector
$\boldsymbol{\tau}_{act}$	Forces and moments from actuators
$\boldsymbol{\tau}_{env}$	Environmental forces and moments
$\boldsymbol{\tau}_{env}^{MD}$	Mean drift force component of environmental force

$\boldsymbol{\tau}_{env}^{WF}$	Excitation force component of environmental force
$\boldsymbol{\tau}_{FF}$	Feed forward term of the commanded control force
$\boldsymbol{\tau}_{max}$	Maximum control force
$\boldsymbol{\tau}_{min}$	Minimum control force
$\boldsymbol{\tau}_{PID}$	PID term of the commanded control force
$\boldsymbol{\tau}_{thr}^{t}$	Thrust in the local thruster frame
$\boldsymbol{\tau}_{thr}^{k}$	Forces and moments from one thruster in the vehicle body frame
$\tilde{\boldsymbol{\eta}}$	Position error
$\boldsymbol{\xi}$	Wave model vector
$\boldsymbol{K}_{anti}$	Anti windup coefficient matrix
$\hat{\mathbf{b}}$	bias estimate vector
$\tilde{\mathbf{y}}$	Observer measurement error
$\mathbf{A}_w$	Wave model system matrix
$\mathbf{A}_w$	wave system matrix
$\mathbf{b}$	Bias vector
$\mathbf{C}$	wave measurement matrix
$\mathbf{C}_w$	Wave model measurement matrix
$\mathbf{D}$	Complete damping matrix
$\mathbf{D}_L$	Linear damping matrix
$\mathbf{D}_{NL}$	Nonlinear damping matrix
$\mathbf{E}_b$	Bias scaling matrix
$\mathbf{H}(s)$	Fluid memory effect transfer function matrix
$\mathbf{K}$	Thrust force coefficient matrix
$\mathbf{K}_d$	Derivative gain matrix
$\mathbf{K}_i$	Integral gain matrix

$\mathbf{K}_p$	Proportional gain matrix
$\mathbf{R}_c$	Rotation matrix for the current
$\mathbf{r}_t$	Position of thruster with regards to center of origin of vehicle
$\mathbf{S}_c$	Skew symmetric matrix for current
$\mathbf{T}$	positive wave filter constants
$\mathbf{T}_b$	Bias time constant matrix
$\mathbf{T}_{con}$	Thruster configuration matrix
$\mathbf{u}$	Thruster control input vector
$\mathbf{w}_b$	Bias white noise
$\mathbf{w}_w$	Wave model noise
$\delta\boldsymbol{\nu}$	Velocity perturbation from the seakeeping frame
$\delta\theta_t$	Perturbation angle of the thruster
ϵ_i	Phase angle for wave component i
$\hat{\nu}$	velocity estimate vector
λ	Wave length
λ_s	Length ratio between full scale and model
$\mathbf{A}_{ii}$	Sub matrix of the complete added mass matrix
$\mathbf{C}_A(\boldsymbol{\nu})$	Hydrodynamic Coriolis and centripetal matrix
$\mathbf{C}_{RB}$	Rigid-body Coriolis and centripetal matrix
$\mathbf{f}_b^b$	Buoyancy force
$\mathbf{f}_g^b$	Gravitational force
$\mathbf{M}_A$	Added mass matrix
$\mathbf{M}_{RB}$	Rigid body mass matrix
$\mathbf{p}_{b/n}^n$	Position in the NED frame
$\mathbf{r}_b^b$	Position of center of buoyancy with regards to the center of origin

∇	Volume of the vessel
ω_i	Wave frequency of wave component i
ϕ	Rotation around NED north-axis
ϕ_t	Polar attitude angle of thruster
ψ	Rotation around NED north-axis
θ	Rotation around NED north-axis
θ_t	Azimuthal attitude angle of thruster.
ζ_n	Signal noise amplitude
$Aii(\omega)$	Frequency dependent coefficient of the added mass matrix
B	Down-component of the buoyancy force
D	Diameter of propeller
F_i^{MD}	Mean drift load in i direction
F_i^{WF}	First order wave load in i direction
J_a	Advance ratio
k	Wave number
K_Q	Torque coefficient
K_T	Thrust coefficient
L_f	Characteristic length of full scale vehicle
L_m	Characteristic length of full model
n	Rotational speed
Q	Torque
$S(\cdot)$	Skew symmetric matrix
T	Thrust
U	Total speed
V_a	Inflow velocity

W	Down-component of the gravitational force
w_n	Zero mean gaussian white noise
x_n	Signal with measurement noise
x_{st}	State from simulation
σ_w	Depth-scaling parameter for the wave loads
AUV	Autonomous Underwater Vehicle
BODY	Body fixed reference frame
CAD	Computer Aided Design
CB	Center of Buoyancy
CG	Center of Gravity
CPM	Control Plant Model
DOF	Degree Of Freedom
DP	Dynamic Positioning
g	Gravitational constant
h	Wave height
KC	Kulegan-Carpenter Number
LF	Low frequency
NED	North-East-Down reference frame
ODE	Ordinary Differential Equations
OOP	Object Oriented Programming
p	Angular velocity around BODY x-axis
PPM	Process Plant Model
q	Angular velocity around BODY y-axis
r	Angular velocity around BODY z-axis
ROV	Remotely Operated Vehicle

RPM	Revolutions Per Minute
u	Velocity along BODY x-axis
UUV	Unmanned Underwater Vehicle
v	Velocity along BODY y-axis
VOC	Vessel Operation Condition
w	Velocity along BODY z-axis
WF	Wave frequency
x	Position along north-axis in the NED frame
y	Position along north-axis in the NED frame
z	Position along north-axis in the NED frame
ZOH	Zero Order Hold

Chapter 1

Introduction

1.1 Background and motivation

In Norway the seafood industry is according to [Nortrade, 2009] one of the most important export products after oil, gas and metal. It accounts to NOK 39.1 billion or 4% of Norway's total export revenues. About NOK 20.2 billion of this comes from farmed fish. The farmed fish are usually raised in large, sea based plants consisting of a ring of floating material at the sea surface and a large, underwater cage usually made of a flexible material as for instance polyamide or polyester.

In the rules and regulations for fish farming, daily inspection of the net is mandatory in order to discover damages and fish escapes early so measures can be taken to prevent further harm. This daily inspection is usually performed by traversing the floating ring at the surface looking for irregularities such as net ruptures in the upper part of the net or even observation of number of fish. The reasons for the ruptures of the net are often due to human error. During the operation of giving medicine to the fish, the net is raised such that a tarpaulin or cover can be used to enclose the fish in a smaller volume. Then the medicine is added to the water and after a while the enclosure is removed and the net is lowered. It is during this raising and lowering the net is most exposed to damaging actions, but damages due to impact of service vessel when berthing also occur. Other reasons for damage can be drifting wood or garbage brought by the ocean currents. The aquaculture-industry in Norway have big problems concerning escape of fish from sea based fish farms. Because the nets go 20-30 meters down into the ocean, damage to the net is easily overlooked. This causes thousands or even hundreds of thousands of fish escape each year. These net damages can be severe in respect of escapes, especially for shoaling species such as salmon, because the shoal often follows if a small amount of fish finds the hole, resulting in large scale escape. To prevent such escapes the cages are also controlled when there is probable cause to suspect rupture. Another large problem is the marine growth on the net itself, causing the

throughput of oxygen rich water to decrease and thereby lowering the welfare and well-being of the fish. This usually causes the fish to grow less and the economy in the fish farming is reduced. In addition to the indirect economical losses, the increased cross section of the net causes higher loads on the structure and its mooring system, which again increase the probability of ruptures and fractures. To accommodate these problems Remotely Operated Vehicles (ROVs) are usually used to clean and inspect the net and if ruptures or fractures are found a diver is put into the water to fix it. During the never ending attempt to minimize the expenses it has been proposed to use ROVs capable of autonomously traversing the net with a cleaning device and inspect the net at the same time. In addition, it is also desirable that the ROV is capable of performing autonomous repairs if damage to net is detected. It is on this proposed solution this thesis is based.

1.1.1 Autonomous Underwater Vehicles

Autonomous Underwater Vehicles (AUVs) are traditionally used to autonomously traverse a predefined path, typically along a pipeline on the sea bottom. Because of large water depths the AUV is thus not affected by the waves, or at least the wave influence is not critical to the operation. They are preprogrammed to perform certain tasks, and carry their own power supply. Usually this power supply is high capacity battery. To increase the battery life, most AUVs are hydrodynamically shaped to minimize drag.

1.1.2 ROV

Remotely Operated Vehicles are Unmanned Underwater Vehicles (UUV) that are controlled from an operator in a control room at the surface through a cable. This cable carries different signals power. They are typically used in offshore industry to perform tasks that are difficult of impossible to conduct by a diver due to the water depth or other hazardous environment. Several types of ROVs exist, from small shoebox-sized ones with a few sensors to large heavy work class ROVs equipped with high-tech sensors and tools to perform work at the seabottom. Because they are supplied with power, they do not have to be hydrodynamically shaped, usually making them from a buoyancy element, shaped as a box, with an aluminum or steel frame underneath containing all sensors and tools.

1.1.3 FhSim - a simulator environment

Write something about the simulator tellering the reader that the models of the environment with waves, current, bottom topography and a single fish cage are given by SINTEF. The simulator is based on an object oriented structure such the implementation will be done the same way. Using a dynamic fish cage model to

simulate the fish cage based on bottom topography, wind, waves and current an approximation of the shape can be used.

1.1.4 Todays solution

The industry has long been looking for a fast and cost-efficient method for net-integrity check, because the current method is based on ROV's or human divers. A single fish net is typically about 120m in circumference and 15-30 meters deep. This gives the ROV-operator or diver an area of about 3600m^2 to check, which is time consuming and thus expensive. Using UUVs with autonomic capabilities this task can be automated and to a large extent be performed without constant supervision. The problem is that the UUV has to navigate at a relatively constant distance with a constant angle to the net, and when influenced by waves and current this can be difficult. Another major concern it that the net is constantly changing shape, making the navigation difficult because it can be difficult to generate a reasonable trajectory. To evaluate the feasibility of the suggested solution, time-domain simulations can be used. In order to do this a high fidelity process plant model for the ROV is thus to be developed.

1.1.5 Previous work

A maneuvering model for a transit type AUV has been developed in [Refsnes, 2007]. This introduces the time derivative of relative velocity added mass force.

[Fossen, 2011] and [Sørensen, 2010] contains lots of literature on how to model marine systems and marine vessel. They also contain control system theory that are used in this thesis. Fossen has made a unified model based on Cummins equation, and in [Fossen and Perez, 2011] made the Matlab add-ins MSS Toolbox and MSS FDI Toolbox. These can be used to calculate the fluid memory transfer functions and process other necessary data for the model.

1.2 Contributions

In Chapter 2 a model for an ROV in the wave zone is developed using a unified approach combining maneuvering and seakeeping theory.

In Chapter 4 a guidance system for traversing a set of dynamic points on a fish cage is described.

The models developed in this thesis has been added to the model library of Fh-Sim.

1.3 Outline of thesis

Chapter 2 provides a six degrees of freedom (DOF) model of a general vessel operating in waves. Environmental loads will also be explained. UUV specific additions will be added and explained.

Chapter 3 will describe the ROV used in this thesis and give an outline of how the vehicle specific coefficients are found.

Chapter 4 provides a description of a general control system with the different parts, in addition to the specifics implemented.

Chapter 5 provides an overview of the environment used for simulations. Object oriented programming and class diagram of the system will be introduced shortly.

Chapter 6 describes the simulations performed by the implemented system.

Chapter 2

Marine vessel modelling

A general model of a vehicle will be developed in this chapter. The dynamics of all marine vessels and vehicles in general have the same main characteristics. According Newton's second law of motion, forces on a mass imposes an acceleration. Thus, the motions of a marine craft can be described by the same fundamental equation. The dynamics of the vehicle is divided into *kinematics* and *kinetics*. The kinematics considers the geometrical aspects of the motion of the vehicle like representation of the motions in different coordinate systems while the kinetics concerns the forces and moments involved.

> *The study of ship dynamics has traditionally been covered by two main theories:* maneuvering *and* seakeeping. *Maneuvering refers to the study of ship motion in absence of wave excitation (calm water). (...) Seakeeping, on the other hand, refers to the study of motion of a marine craft on constant course and speed when there is wave excitation.*
>
> [Fossen, 2011]

Process plant models for vessels are typically developed with the assumption of calm water so that the maneuvering theory can be used. Using this assumption all coefficients are constant. In the case for this thesis a general vessel operating in an environment with waves, such that a *unified* approach where the combined seakeeping and maneuvering theory is used. This allows for time-domain simulations of a vessel in at constant speed in waves. In addition, the assumption of linear superposition is made, such that wave induced forces for different speeds and sea states can be added. The same assumption is made for nonlinear damping and restoring forces resulting in a unified model combining the most significant terms of both maneuvering and seakeeping.

The seakeeping theory refers to the study of ship motions when there is wave excitation and the craft keeps its heading and speed constant[Fossen, 2011]. This introduces a dissipative force called *fluid memory effects*. The theory is formulated

using seakeeping axes {s} where the state vector represents the perturbations with respect to a fixed equilibrium state.

2.1 Kinematics

2.1.1 Reference frames

When modelling a craft in 6 DOF it is convenient to define the reference frames as in [Fossen, 2011].

NED The earth-fixed frame is denoted as North-East-Down. This frame is usually defined as the tangent plane on the surface of the earth. The x-coordinate points north, the y-coordinate points east and the z-coordinate points down. For navigation in a small area with approximately the same longitude and latitude, *flat earth navigation*, the NED-frame is considered as inertial. Position and attitude are expressed in this frame.

BODY The body-fixed reference frame is a moving coordinate frame fixed to the vessel, where the x-axis points from aft to fore, y-axis directed starboard(right) and z-axis pointing from top to bottom. The linear and angular velocities are expressed in this frame.

To model the vessel dynamics the formulation presented in [SNAME, 1950] is used.

Table 2.1: The notation of SNAME for marine vessels

DOF		Linear and angular velocity	Position and Euler angles
1	Surge	u	x
2	Sway	v	y
3	Heave	w	z
4	Roll	p	ϕ
5	Pitch	q	θ
6	Yaw	r	ψ

Using the notation in [Fossen, 2011], the kinematics can be described in a vectorial notation as following:

NED position	$\mathbf{p}^n_{b/n} =$	$[x, y, z]^\top \in \mathbb{R}^3$
Attitude (Euler Angles)	$\boldsymbol{\Theta}_{bn} =$	$[\phi, \theta, \psi]^\top \in \mathcal{S}^3$
Body-fixed linear velocity	$\boldsymbol{\nu}^b_{b/n} =$	$[u, v, w]^\top \in \mathbb{R}^3$
Body-fixed angular velocity	$\boldsymbol{\omega}^b_{b/n} =$	$[p, q, r]^\top \in \mathbb{R}^3$
Forces and moments	$\boldsymbol{\tau} =$	$[X\ Y\ Z\ K\ M\ N]^\top \in \mathbb{R}^6$

where $\mathbb{R}^3$ is the Euclidean space of dimension three and $\mathcal{S}^3$ denotes a sphere defined by three angles on the interval $[0, 2\pi]$. The general motion for a marine craft in 6DOF is thus described by the following vectors:

$$\boldsymbol{\eta} = \begin{bmatrix} \mathbf{p}_{b/n}^n \\ \boldsymbol{\Theta}_{nb} \end{bmatrix}, \qquad \boldsymbol{\nu} = \begin{bmatrix} \mathbf{v}_{b/n}^b \\ \boldsymbol{\omega}_{nb} \end{bmatrix}$$

where:

$\mathbf{p}_{b/n}^n$: position of body frame with respect to NED frame expressed in NED frame.

$\boldsymbol{\nu}_{b/n}^b$: linear velocity of body frame with respect to NED-frame expressed in body frame.

$\boldsymbol{\tau}$: Forces and moments acting on the craft in the body-fixed frame.

The kinematic relation between the body-fixed velocity $\boldsymbol{\nu}$ and the position $\boldsymbol{\eta}$ in NED-frame is expressed as:

$$\dot{\boldsymbol{\eta}} = \mathbf{J}(\boldsymbol{\Theta}_{nb})\boldsymbol{\nu} \tag{2.1}$$

where $\mathbf{J}(\boldsymbol{\Theta}_{nb}) \in \mathbb{R}^{6\times 6}$ is the transformation matrix given as:

$$\mathbf{J}(\boldsymbol{\Theta}_{nb}) = \begin{bmatrix} \mathbf{R}(\boldsymbol{\Theta}_{nb}) & \mathbf{0}_{3\times 3} \\ \mathbf{0}_{3\times 3} & \mathbf{T}(\boldsymbol{\Theta}_{nb}) \end{bmatrix}$$

The matrices $\mathbf{R}(\boldsymbol{\Theta}_{nb})$ and $\mathbf{T}(\boldsymbol{\Theta}_{nb})$ are given as:

$$\mathbf{R}(\boldsymbol{\Theta}_{nb}) = \begin{bmatrix} c\psi c\theta & -s\psi c\phi + c\psi s\theta s\phi & s\psi s\phi + c\psi c\phi s\theta \\ s\psi c\theta & c\psi c\phi + s\phi s\theta s\psi & -c\psi s\phi + s\theta s\psi c\phi \\ -s\theta & c\theta s\phi & c\theta c\phi \end{bmatrix}$$

$$\mathbf{T}(\boldsymbol{\Theta}_{nb}) = \begin{bmatrix} 1 & s\phi t\theta & c\phi t\theta \\ 0 & c\phi & -s\phi \\ 0 & s\phi/c\theta & c\phi/c\theta \end{bmatrix}, \qquad \theta \neq \frac{\pi}{2}$$

where $s(\cdot) = \sin(\cdot)$, $c(\cdot) = \cos(\cdot)$, and $t(\cdot) = \tan(\cdot)$.

2.2 Modelling of vessel kinetics

The kinetics of a marine craft is usually separated into two major parts; rigid-body and hydrodynamic forces and moments.

2.2.1 Rigid-body forces and moments

The rigid body kinetics can be expressed in a vectorial setting according to [Fossen, 2011].

$$\mathbf{M}_{RB}\dot{\boldsymbol{\nu}} + \mathbf{C}_{RB}(\boldsymbol{\nu})\boldsymbol{\nu} = \boldsymbol{\tau} \tag{2.2}$$

where $\mathbf{M}_{RB}$ is the rigid-body mass matrix and $\mathbf{C}_{RB}$ is the rigid-body Coriolis and centripetal matrix due to the rotation of the body frame about the inertial frame. These matrices contain coefficients that can be determined based on gravity and the inertial properties of the vehicles. The representation of $\mathbf{M}_{RB}$ is unique and satisfies

$$\mathbf{M}_{RB} = \mathbf{M}_{RB}^{\top} > 0, \qquad \dot{\mathbf{M}}_{RB} = \mathbf{0}_{6\times 6}$$

where

$$\mathbf{M}_{RB} = \begin{bmatrix} \mathbf{M}_{11} & \mathbf{M}_{12} \\ \mathbf{M}_{21} & \mathbf{M}_{22} \end{bmatrix} = \begin{bmatrix} m & 0 & 0 & 0 & mz_g & -my_g \\ 0 & m & 0 & -mz_g & 0 & mx_g \\ 0 & 0 & m & my_g & mx_g & 0 \\ 0 & -mz_g & my_g & I_x & -I_{xy} & -I_{xz} \\ mz_g & 0 & -mx_g & -I_{yx} & I_y & -I_{yz} \\ -my_g & mx_g & 0 & -I_{zx} & -I_{zy} & I_z \end{bmatrix}$$

Here $\mathbf{r}_g^b := [x_g, y_g, z_g]^{\top}$ is the position of the Center of Gravity (CG) with respect to the body-frame origin. According to [Fossen and Fjellstad, 1995] the Coriolis-centripetal matrix can be parameterized such that $\mathbf{C}_{RB}(\boldsymbol{\nu}) = -\mathbf{C}_{RB}^{\top}(\boldsymbol{\nu})$ by choosing

$$\mathbf{C}_{RB}(\boldsymbol{\nu}) = \begin{bmatrix} \mathbf{0}_{3\times 3} & -\mathbf{S}(\mathbf{M}_{11}\boldsymbol{\nu}_1 + \mathbf{M}_{12}\boldsymbol{\nu}_2) \\ -\mathbf{S}(\mathbf{M}_{11}\boldsymbol{\nu}_1 + \mathbf{M}_{12}\boldsymbol{\nu}_2) & -\mathbf{S}(\mathbf{M}_{21}\boldsymbol{\nu}_1 + \mathbf{M}_{22}\boldsymbol{\nu}_2) \end{bmatrix}$$

where $\boldsymbol{\nu}_1 = \mathbf{v}_{b/n}^b$, $\boldsymbol{\nu}_2 = \boldsymbol{\omega}_{b/n}^b$ and $\mathbf{S}$ is the skew symmetric matrix

$$\mathbf{S}([a,b,c]) = \begin{bmatrix} 0 & -c & b \\ c & 0 & -a \\ -b & a & 0 \end{bmatrix}$$

2.2.2 Hydrodynamic forces and moments

In this section some of the factors concerning the hydrodynamic forces will be modelled and discussed. In section 2.7 some of the factors which have been left out is explained shortly.

The hydrodynamic forces and moments are contained in the vector $\boldsymbol{\tau}$ in (2.2) given as

$$\boldsymbol{\tau} = -\mathbf{M}_A\dot{\boldsymbol{\nu}} - \mathbf{C}_A(\boldsymbol{\nu})\boldsymbol{\nu} - \mathbf{D}(\boldsymbol{\nu})\boldsymbol{\nu} - \mathbf{g}(\boldsymbol{\eta}) + \boldsymbol{\tau}_{env} + \boldsymbol{\tau}_{act} \tag{2.3}$$

where the different terms will be discussed in the following sections.

Added mass and Coriolis-centripetal matrices

As a vehicle oscillates in a fluid the surrounding fluid is forced to oscillate. This induces an oscillating pressure on the body surface. Integrating this pressure over the body surface gives resulting forces and moments on the body. These forces and moments are called added mass and damping loads and are dependent on the frequency of oscillation ω and velocity of the incoming fluid U. The hydrodynamic added mass matrix $\mathbf{M}_A$ is defined as follows

$$\begin{aligned}\mathbf{M}_A &= \begin{bmatrix}\mathbf{A}_{11} & \mathbf{A}_{12}\\ \mathbf{A}_{21} & \mathbf{A}_{22}\end{bmatrix}\\ &= \begin{bmatrix} A11(\omega) & \dots & A16(\omega)\\ \vdots & \ddots & \vdots\\ A61(\omega) & \dots & A66(\omega)\end{bmatrix}\end{aligned}$$

The hydrodynamic Coriolis and centripetal matrix $\mathbf{C}_A(\boldsymbol{\nu})$ consists of vehicle velocities and added mass coefficients and can according to [Fossen, 2011] be parametrized such that it is skew-symmetric:

$$\mathbf{C}_A(\boldsymbol{\nu}) = \begin{bmatrix}\mathbf{0}_{3\times 3} & -\mathbf{S}(\mathbf{A}_{11}\boldsymbol{\nu}_1 + \mathbf{A}_{12}\boldsymbol{\nu}_2)\\ -\mathbf{S}(\mathbf{A}_{11}\boldsymbol{\nu}_1 + \mathbf{A}_{12}\boldsymbol{\nu}_2) & -\mathbf{S}(\mathbf{A}_{21}\boldsymbol{\nu}_1 + \mathbf{A}_{22}\boldsymbol{\nu}_2)\end{bmatrix}$$

Hydrodynamic damping

Modelling of the six DOF hydrodynamic damping forces and moments is a complicated task. The forces and moments are highly speed dependent and there are considerable coupling effects between the degrees of freedom. Using the assumption of linear superposition as in [Fossen, 2011] the hydrodynamic damping can be modelled as a sum of linear and nonlinear damping. This gives

$$\mathbf{D}(\boldsymbol{\nu})\boldsymbol{\nu} = \mathbf{D}_L\boldsymbol{\nu} + \mathbf{D}_{NL}(\boldsymbol{\nu})\boldsymbol{\nu}$$

where $\mathbf{D}_L\boldsymbol{\nu}$ is a linear damping term and $\mathbf{D}_{NL}(\boldsymbol{\nu})\boldsymbol{\nu}$ is a nonlinear term. The linear and nonlinear damping matrices are described as in [Fossen, 2011]:

$$\mathbf{D}_L = \begin{bmatrix} X_u & \dots & X_r \\ \vdots & \ddots & \vdots \\ N_u & \dots & N_r \end{bmatrix}$$

where the coefficients are constant and

$$\mathbf{D}_{NL} = \begin{bmatrix} X_{|u|u}|u| & \dots & X_{|u|r}|u| \\ \vdots & \ddots & \vdots \\ N_{|r|u}|r| & \dots & N_{|r|r}|r| \end{bmatrix}$$

The influence of body symmetry on system matrices

Symmetric properties of the vehicle can be utilized to simplify some of the matrices. Added mass, viscous damping, and the matrix for fluid memory effect can be simplified.

In case of bottom-top symmetry a six degree of freedom added mass matrix typically looks like

$$\mathbf{M}_A = \begin{bmatrix} A11 & A12 & 0 & 0 & 0 & A16 \\ A21 & A22 & 0 & 0 & 0 & A26 \\ 0 & 0 & A33 & A34 & A35 & 0 \\ 0 & 0 & A43 & A44 & A45 & 0 \\ 0 & 0 & A53 & A54 & A55 & 0 \\ A61 & A62 & 0 & 0 & 0 & A66 \end{bmatrix} \tag{2.4}$$

In case of port-starboard symmetry the matrix becomes

$$\mathbf{M}_A = \begin{bmatrix} A11 & 0 & A13 & 0 & A15 & 0 \\ 0 & A22 & 0 & A24 & 0 & A26 \\ A31 & 0 & A33 & 0 & A35 & 0 \\ 0 & A42 & 0 & A44 & 0 & A46 \\ A51 & 0 & A53 & 0 & A55 & 0 \\ 0 & A62 & 0 & A64 & 0 & A66 \end{bmatrix} \tag{2.5}$$

In case of fore-aft symmetry the matrix is

$$\mathbf{M}_A = \begin{bmatrix} A11 & 0 & 0 & 0 & A15 & A15 \\ 0 & A22 & A23 & A24 & 0 & 0 \\ 0 & A32 & A33 & A34 & 0 & 0 \\ 0 & A42 & A43 & A44 & 0 & 0 \\ A51 & 0 & 0 & 0 & A55 & A56 \\ A61 & 0 & 0 & 0 & A65 & A66 \end{bmatrix} \tag{2.6}$$

If the vessel has both aft-fore and port-starboard symmetry the matrix becomes

$$\mathbf{M}_A = \begin{bmatrix} A11 & 0 & 0 & 0 & A15 & 0 \\ 0 & A22 & 0 & A24 & 0 & 0 \\ 0 & 0 & A33 & 0 & 0 & 0 \\ 0 & A42 & 0 & A44 & 0 & 0 \\ A51 & 0 & 0 & 0 & A55 & 0 \\ 0 & 0 & 0 & 0 & 0 & A66 \end{bmatrix} \tag{2.7}$$

In the last case where the vessel has symmetry in aft-fore, port-starboard and top-bottom the resulting matrix becomes:

$$\mathbf{M}_A = \begin{bmatrix} A11 & 0 & 0 & 0 & 0 & 0 \\ 0 & A22 & 0 & 0 & 0 & 0 \\ 0 & 0 & A33 & 0 & 0 & 0 \\ 0 & 0 & 0 & A44 & 0 & 0 \\ 0 & 0 & 0 & 0 & A55 & 0 \\ 0 & 0 & 0 & 0 & 0 & A66 \end{bmatrix} \tag{2.8}$$

2.2.3 Actuator forces

The actuator forces are highly vessel dependent because different vessels may have different outfitting. Therefore this section will describe a basic thruster which is rotatable in the body frame x-y plane.

The relationship between thrust and torque from the propeller is given in [Sørensen, 2010] as

$$T = \text{sign}(n) K_T \rho D^4 n^2 \tag{2.9}$$

$$Q = \text{sign}(n) K_Q \rho D^5 n^2 \tag{2.10}$$

where T and Q are thrust and torque produced, n is revolutions per second, ρ is water density, D is propeller diameter and K_T and K_Q are thrust- and torque coefficients dependent of the advance ratio J_a. The advance ratio is given as the ratio between the distance traveled during one revolution and the propeller diameter and is expressed as

$$J_a = \frac{V_a}{nD} \tag{2.11}$$

where V_a is the propeller inflow velocity. The thrust in (2.9) is the thrust produced in the thruster frame, in the axial direction of the propeller and has to be transformed into the body frame. The attitude of the thruster with regard to body axis is assumed to be given as the two angles θ_t and ϕ_t, like in mathematical spherical coordinates. θ_t is the azimuthal angle from body frame x-axis in the x-y plane while ϕ_t is the polar angle from the body z-axis. The position of the thruster in body coordinates with regard to the center of origin of the vehicle is given as $\mathbf{r}_t = [x_t, y_t, z_t]$. The thrust from one thruster in its thruster frame is given as

$$\boldsymbol{\tau}_{thr}^{t} = \begin{bmatrix} T \\ 0 \\ 0 \end{bmatrix}$$

The relation between the axial thrust and thrust in the body frame is given by using the transformation matrix $\mathbf{R}(0, \phi_t, \theta_t + \delta\theta_t)$ where $\delta\theta_t$ is the optional rotated angle for a rotatable thruster:

$$\boldsymbol{\tau}_{thr}^{XYZ} = \mathbf{R}\boldsymbol{\tau}_{thr}^{t} \tag{2.12}$$

Using the position of the thruster the forces and moments from thruster k on the vehicle can be expressed as

$$\boldsymbol{\tau}_{thr}^{k} = \begin{bmatrix} (\boldsymbol{\tau}_{thr}^{XYZ})^{\top} \\ (\mathbf{r}_t \times \boldsymbol{\tau}_{thr}^{XYZ})^{\top} \end{bmatrix} \tag{2.13}$$

Thrust losses

The thrust from a thruster is influenced by a number of factors, causing the efficiency to decrease. Some of these factors are

- *Thruster-thruster interaction* is as indicated interaction between different thrusters. If the wake of one thruster intersect the inflow or wake of another thruster, the efficiency on both thrusters decreases. In the case of rotatable thrusters this can be prevented using forbidden zones.
- *Thruster-hull interaction* is the case when the hull interacts with the inflow or wake of the thruster. If the wake is near the hull the wake is sucked to the hull and the efficiency decreases. This is called the "Coanda effect".

To model such thrust losses a thrust factor t is used, so that the thrust from each thruster is given as:

$$\boldsymbol{\tau}_{thr}^{t} = \begin{bmatrix} T(1-t_t) \\ 0 \\ 0 \end{bmatrix} \tag{2.14}$$

Thruster dynamics

The dynamic behavior of the thrusters are modelled using a first order filter given in [Sørensen, 2010] to introduce a phase lag between the input rpm command and the actual rpm as:

$$\dot{n}_i = -\frac{1}{T_i}(n_i - n_c) \tag{2.15}$$

where n_i is the rotational velocity [rpm] of thruster i, T_i is the thruster i time constant and n_c is the commanded rpm.

2.3 Modelling of environment

2.3.1 Wave loads

When an underwater vehicle is operating in an area with waves and at a depth $z < \frac{\lambda}{2}$,where λ is the wave length, the vehicle is considered to be operating in the wave zone and thus affected by the waves. It is assumed that the wave loads are based on potential theory where viscous effects are neglected. Using linear wave-frequency model as described in [Faltinsen, 1990], the wave loads are devided into *wave reaction* and *wave excitation*. These two contributions added together amounts to the total wave force. They are defined as

Wave reaction Forces and moments on the body when the structure is forced to oscillate with the wave excitation frequency in any rigid body mode. There are no incident waves. The hydrodynamic loads are identified as *added mass*, *damping* and *restoring* terms.

Wave excitation Forces and moments on the body when the structure is restrained from oscillating and there are incident regular waves. The hydrodynamic loads are called *wave excitation loads* and composed of so-called Froude-Krylov and diffraction forces and moments.

Froude Krylov are forces and moments due to the undisturbed pressure in the fluid as if the vessel is not there. The diffraction forces and moments are because the pressure field changes due to the existence of the vessel.

As mentioned in the beginning of chapter 2 these forces and moments are expressed in the hydrodynamic seakeeping frame. The origin of this frame lies in the mean position of the vessel with the x-axis fore, y-axis port and z-axis up.

Wave reaction

According to [Faltinsen, 1990] added mass and damping loads are steady-state hydrodynamic forces and moments due to forced harmonic rigid body motions.

There are no incident waves. Forced motions results in oscillating fluid pressures on the body surface. By integrating this fluid pressure over the body the added mass forces and moments are found. It has been shown that these forces and moments are highly dependent on body geometry, frequency of oscillation and vessel speed.

By simple energy considerations it is easy to imagine that a vessel in forced oscillations produces waves. In these waves there is energy that is dissipated from the system when the waves travels outwards. This dissipation is frequency dependent and called potential damping.

Wave excitation

Because AUVs and ROVs are relatively small in size compared to the wave length, the wave loads can usually be approximated by integrating the dynamic pressure caused by the wave-potential over the hull. The wave loads are typically split into second order low frequency or constant mean drift loads proportional with the squared wave amplitude, and high frequency first order wave loads proportional with the wave amplitude to the power of one. According to [Faltinsen, 1990] the mean drift wave loads due to several regular wave components with frequency ω_i can be expressed as

$$F_i^{MD} = \sum_{j=1}^{N}\sum_{k=1}^{N} A_j A_k (T_{jk}^{ic} \cos\{(\omega_k - \omega_j)t + (\epsilon_k - \epsilon_j)\} + T_{jk}^{is} \sin\{(\omega_k - \omega_j)t + (\epsilon_k - \epsilon_j)\}) \quad (2.16)$$

where N is the number of wave components, A_i is the wave component amplitude,ϵ_i is a random phase angle, and T_{jk}^{ic} and T_{jk}^{is} are coefficients interpreted as second-order transfer functions for difference frequency loads.

The first order wave frequency (WF) loads are given by

$$F_i^{WF} = F_i \mathrm{e}^{-i(\omega t + \epsilon_i)} \quad (2.17)$$

where F_i^{WF} is the force or moment in i-direction and F_i are the complex amplitude in i-direction of the exciting forces and moments and ϵ_i the phase angle.

For a more thorough description the readers are advised to
read [Newman, 1977] or [Faltinsen, 1990].

Due to the small size of the ROV compared to the wavelength it can be assumed that the diffraction forces can be neglected, such that the total excitation forces and moments is found from Froude-Krylov alone.

A simplified alternative to this approach is given in [Sørensen, 2010]. This approximation is based on the assumption that the sea state is constant during the period

of simulation such that the slowly varying wave loads can be expressed as a bias with constant coefficients as

$$\dot{\mathbf{b}} = -\mathbf{T}_b^{-1}\mathbf{b} + \mathbf{E}_b\mathbf{w}_b$$

where $\mathbf{b} \in \mathbb{R}^6$ is the bias vector, $\mathbf{w} \in \mathbb{R}^6$ a zero mean Gaussian white noise vector, $\mathbf{T}_b \in \mathbb{R}^{6\times6}$ a diagonal matrix of bias time constants and $\mathbf{E}_b \in \mathbb{R}^{6\times6}$ a diagonal scaling matrix. The wave-frequency component of the wave loads with constant coefficients can be expressed as an excitation in position according to

$$\dot{\boldsymbol{\xi}} = \mathbf{A}_w\boldsymbol{\xi} + \mathbf{E}_w\mathbf{w}_w \tag{2.18}$$

$$\boldsymbol{\eta}_w = \mathbf{C}_w\boldsymbol{\xi} \tag{2.19}$$

where $\boldsymbol{\xi} \in \mathbb{R}^{12}$ is the wave model states, $\mathbf{A}_w \in \mathbb{R}^{12\times12}$ is the system matrix, $\mathbf{E}_w \in \mathbb{R}^{12\times6}$ the disturbance matrix, $\mathbf{w}_w \in \mathbb{R}^6$ a Gaussian white noise vector and $\mathbf{C}_w \in \mathbb{R}^{6\times12}$ is the measurement matrix.

Depth dependence of the wave loads

According to [Faltinsen, 1990] the dynamic pressure in the fluid decreases with increasing water depth such that the wave loads can be scaled with the following scaling function to compensate for depth changes

$$\sigma(k, z) = \exp(-kz) \tag{2.20}$$

where k is the wave number,z is the depth of the vehicle and it is assumed infinite water depth.

2.3.2 Current

According to [Fossen, 2011] the slowly varying current load is usually modelled by simply changing the vehicle velocity vector $\boldsymbol{\nu}$ used when calculating the hydrodynamic loads with the relative velocity expressed as

$$\boldsymbol{\nu}_r = \boldsymbol{\nu} - \boldsymbol{\nu}_c$$

where $\boldsymbol{\nu}_c$ is the current velocity given in body frame. The current is usually given in the NED-frame as $\boldsymbol{\nu}_c^n$ so it has to be transformed into the body frame. Assuming that the current is irrotational it can be expressed as $\boldsymbol{\nu}_c^n = [u_c\ v_c\ w_c\ 0\ 0\ 0]^\top$. The velocity vector in the body frame can thus be described as

$$\boldsymbol{\nu}_c = \text{diag}\left[\mathbf{R}(\boldsymbol{\Theta})^\top, \mathbf{0}_{3\times3}\right]\boldsymbol{\nu}_c^n$$

2.4 Hydrostatic forces

The hydrostatic restoring forces denoted as $\mathbf{g}(\boldsymbol{\eta})$ in (2.3) depends highly on the type of vessel. There are restoring forces and moments for surface vessels and other forces and moments for underwater vehicles. As this thesis deals with an ROV, the restoring forces for underwater vehicles are treated in Section 3.

2.5 Process plant model for a marine vessel

Maneuvering model

Using the equations described above and denoting the slowly varying wave loads as $\boldsymbol{\tau}_{env}^{MD}\sigma$ where

$$\boldsymbol{\tau}_{env}^{MD} = \begin{bmatrix} F_1^{MD} & F_2^{MD} & F_3^{MD} & F_4^{MD} & F_5^{MD} & F_6^{MD} \end{bmatrix}^\top$$

we get the following low frequency process plant model for a general vessel:

PPM1:

$$\dot{\boldsymbol{\eta}} = \mathbf{J}(\boldsymbol{\eta})\boldsymbol{\nu} \tag{2.21a}$$

$$\begin{aligned} \mathbf{M}\dot{\boldsymbol{\nu}} + \mathbf{C}_{RB}(\boldsymbol{\nu})\boldsymbol{\nu} = &- \mathbf{C}_A(\boldsymbol{\nu}_r)\boldsymbol{\nu}_r - \mathbf{D}_L\boldsymbol{\nu}_r \\ &- \mathbf{D}_{NL}(\boldsymbol{\nu}_r)\boldsymbol{\nu}_r - \mathbf{g}(\boldsymbol{\eta}) + \boldsymbol{\tau}_{env}^{MD}\sigma + \boldsymbol{\tau}_{act} \end{aligned} \tag{2.21b}$$

It must be noted that the hydrodynamic coefficients in this model are constant, i.e the added mass is $\mathbf{M}_A(\omega) = \mathbf{M}_A(\infty)$.

It is also possible to add the synthetic wave model described in 2.18 - 2.19 to this model without violating the assumptions made, because this only affects the measurement of the position.

Unified model

When including high frequency loads such as waves, the maneuvering model has to be changed. In [Fossen, 2011] this is done using a unified approach. This is based on the work done in [Cummins, 1962] and [Ogilvie, 1964]. By denoting the perturbed velocities in the seakeeping frame as $\delta\boldsymbol{\nu}$, a *fluid memory effect* can be approximated by matrix $\mathbf{H}(s)$ containing relative degree one transfer functions such that

$$\boldsymbol{\mu} = \mathbf{H}(s)\delta\boldsymbol{\nu}$$

where the transfer functions in $\mathbf{H}(s)$ are found using WAMIT-results and MSS FDI Toolbox [Fossen and Perez, 2011]. The structure of the transfer function matrix is

$$\mathbf{H}(s) = \begin{bmatrix} f_{11}(s) & \dots & f_{16}(s) \\ \vdots & \ddots & \vdots \\ f_{61}(s) & \dots & f_{66}(s) \end{bmatrix} \tag{2.22}$$

Introducing the fluid memory effect as a frequency-domain model results in a model containing both time and frequency. To make the process plant model a true time-domain model it is possible to approximate the transfer functions for the fluid memory effect as statespace models:

$$\dot{\mathbf{x}} = \mathbf{A}_r\mathbf{x} + \mathbf{B}_r\delta\boldsymbol{\nu} \tag{2.23}$$
$$\mu_{ij} = \mathbf{C}_r\mathbf{x} \tag{2.24}$$

where μ_{ij} is the state space model for couped fluid memory effect in e.g. surge and sway. This results in the following expressing for the combined fluid-memory effect $\boldsymbol{\mu} \in \mathbb{R}^6$:

$$\boldsymbol{\mu} = \begin{bmatrix} \sum \mu_{1i} \\ \sum \mu_{2i} \\ \sum \mu_{3i} \\ \sum \mu_{4i} \\ \sum \mu_{5i} \\ \sum \mu_{6i} \end{bmatrix} \quad \text{for } i = 1, .., 6 \tag{2.25}$$

It must be stressed that introducing coupled fluid memory effect in all degrees of freedom will increase the computational demand making the simulations slower. If the vehicle has planes of symmetry, (2.22) can be simplified the same way as in (2.4)-(2.8).

If added mass coefficients for the infinite frequency case is used in the the terms containing hydrodynamic coefficients in (2.21) ($\mathbf{C}_A(\boldsymbol{\nu}_r)$ and $\mathbf{M}_A$), a unified model can be expressed as:

PPM2:

$$\dot{\boldsymbol{\eta}} = \mathbf{J}(\boldsymbol{\eta})\boldsymbol{\nu} \tag{2.26a}$$
$$\begin{aligned} \mathbf{M}\dot{\boldsymbol{\nu}} + \mathbf{C}_{RB}(\boldsymbol{\nu})\boldsymbol{\nu} &= -\mathbf{C}_A(\boldsymbol{\nu}_r)\boldsymbol{\nu}_r - \mathbf{D}_L\boldsymbol{\nu}_r \\ &\quad - \mathbf{D}_{NL}(\boldsymbol{\nu}_r)\boldsymbol{\nu}_r - \mathbf{g}(\boldsymbol{\eta}) - \boldsymbol{\mu} + \boldsymbol{\tau}_{env} + \boldsymbol{\tau}_{act} \end{aligned} \tag{2.26b}$$

where both the mean drift and excitation wave loads are in the term $\boldsymbol{\tau}_{env}$

2.6 ROV specific loads

2.6.1 Relative acceleration

In the general model for a marine vessel it is assumed that the angular velocities of the vessel are relatively small. In the case of an ROV, this assumption is usually invalid. Because of the physical size, it is capable of large angular velocities and the influence from the current has to be taken into account. According to [Refsnes, 2007] this can be done in the following manner. By assuming that the current is constant in the NED frame, the time derivative of the relative velocity is given as

$$\dot{\boldsymbol{\nu}}_c = -\mathbf{R}_c^\top(\boldsymbol{\Theta})\dot{\mathbf{R}}_c(\boldsymbol{\Theta})\boldsymbol{\nu}_c$$

where $\mathbf{R}_c \equiv \text{diag}\,[\mathbf{R}(\boldsymbol{\Theta}), \mathbf{0}_{3\times3}]$. Using the fact that $\dot{\mathbf{R}}(\boldsymbol{\Theta}) = \mathbf{R}(\boldsymbol{\Theta})\mathbf{S}(\boldsymbol{\omega})$, the time derivative can be expressed as

$$\dot{\boldsymbol{\nu}}_c = -\mathbf{R}_c^\top(\boldsymbol{\Theta})\mathbf{R}_c(\boldsymbol{\Theta})\mathbf{S}_c(\boldsymbol{\omega})\boldsymbol{\nu}_c = -\mathbf{S}(\boldsymbol{\omega})\boldsymbol{\nu}_c \tag{2.27}$$

where $\mathbf{S}_c(\boldsymbol{\omega}) = \text{diag}\,[\mathbf{S}(\boldsymbol{\omega}), \mathbf{0}_{3\times3}]$. The force due to relative acceleration can then be expressed as

$$-\mathbf{M}_A\dot{\boldsymbol{\nu}}_c = \mathbf{M}_A\mathbf{S}_c(\boldsymbol{\omega})\boldsymbol{\nu}_c \tag{2.28}$$

2.6.2 Hydrostatics

As mentioned, the restoring forces and moments are dependent of type of vessel, and thus this section only applies to underwater vehicles. The gravitational force $\mathbf{f}_g^b$ acts through CG. Similar, the buoyancy force $\mathbf{f}_b^b$ acts through Center of Buoyancy (CB) defined by the vector $\mathbf{r}_b^b := [x_b, y_b, z_b]^\top$. Letting ∇ be the volume of fluid displaced by the vehicle, g the acceleration of gravity(positive downwards) and ρ the density of water, the weight and buoyancy of the body can be written according to [SNAME, 1950] as

$$W = mg, \qquad B = \rho g \nabla \tag{2.29}$$

As these forces acts in the vertical plane of NED, according to [Fossen, 2011] we have

$$\mathbf{f}_g^n = \begin{bmatrix} 0 \\ 0 \\ W \end{bmatrix} \quad \text{and} \quad \mathbf{f}_b^n = -\begin{bmatrix} 0 \\ 0 \\ B \end{bmatrix} \tag{2.30}$$

In the body-frame the buoyancy and gravity force can be expressed as

$$\mathbf{f}_g^b = \mathbf{R}(\boldsymbol{\Theta})^{-1}\mathbf{f}_g^n \tag{2.31}$$

$$\mathbf{f}_b^b = \mathbf{R}(\boldsymbol{\Theta})^{-1}\mathbf{f}_b^n \tag{2.32}$$

The restoring forces and moment can thus be expressed in the body-frame as

$$\mathbf{g}(\boldsymbol{\eta}) = -\begin{bmatrix} \mathbf{R}(\boldsymbol{\Theta})^{-1}(\mathbf{f}_g^n + \mathbf{f}_b^n) \\ \mathbf{r}_g^b \times \mathbf{R}(\boldsymbol{\Theta})^{-1}\mathbf{f}_g^n + \mathbf{r}_b^b \times \mathbf{R}(\boldsymbol{\Theta})^{-1}\mathbf{f}_b^n \end{bmatrix} \tag{2.33}$$

2.6.3 Umbilical

Dependent on the current velocity and the depth of the ROV, the forces and moments due to the umbilical can have a large impact. The current induces a drag force on the cable-run from the surface to the ROV. If the vehicle is suppose to operate at significant depths these loads have to be modelled. Because the ROV in this thesis is supposed to operate at relatively small depths, the umbilical force model is omitted.

2.7 Other influencing, but unmodelled factors

It must be emphasised that the model developed in the previous section omits several factors which influences the model accuracy. Some of the factors omitted in the proposed model will be introduced shortly in the following section. The reasons for omitting most of these factors are because of the complexity of the phenomenon, and that they are difficult to model with desirable accuracy. In other cases the reason is simply to simplify the implementation.

Reynolds number

According to [Berg, 2007] most AUVs and ROVs will be operating in a Reynolds number area where the flow is changing from laminar to turbulent. Because of this varying vessel operation condition (VOC) the viscous damping will be dependent of Reynolds number. This can easily be seen by comparing the drag coefficient (C_D) for a cylinder in laminar and turbulent flow. In laminar flow $C_D^{lam} \approx 1.0$ and in turbulent flow this decreases to $C_D^{turb} \approx 0.3$.

Keulegan–Carpenter number

For an ROV or AUV with small body members, oscillation of the vessel will according to [Berg, 2007] cause the damping to be dependent of the Kulegan-Carpenter (KC) number. If the body oscillates it can be interacting with the vortices shed earlier, which causes the velocity of the incoming flow to be different than vessel relative velocity. This important contribution is not considered in this thesis.[Faltinsen, 1990] contains more about the Keulegan–Carpenter number and its influence on the body motions.

Proximity effects

When the vehicle is operating near the surface or near the sea bottom or another object, an interaction effect can be observed in real life. This is not taken into account.

Wind effects

For a surface vessel, the wind related forces can be significant. Because the main focus of this thesis are an ROV, the wind loads are omitted.

Chapter 3

ROV Argus Mariner

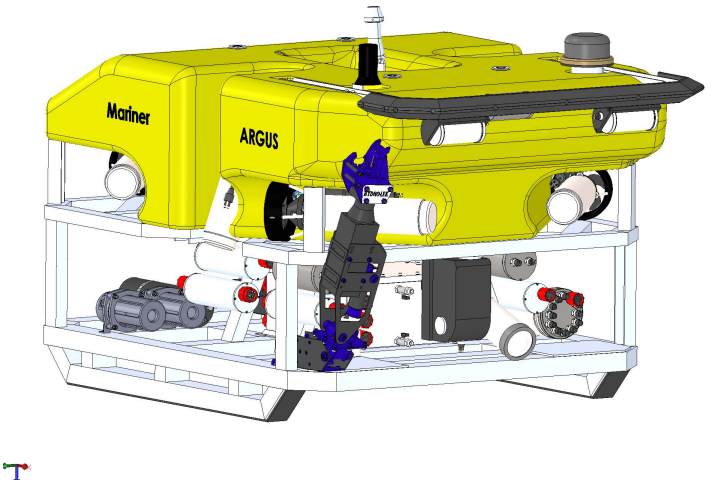

Figure 3.1: CAD drawing of Argus Mariner by Argus Remote Systems

The vehicle modelled in this thesis is the ROV Argus Mariner by Argus Remote Systems AS (Argus) depicted in Figure 3.1. The ROV has been developed as part of a project called "Utvikling av ROV som verktøy for automatiserte simultane not-operasjoner i oppdrettsmerd (MerdROV)" with six participating companies.

Based on a Computer Aided Design (CAD) model provided by Argus Remote Systems and the 3D CAD software SolidWorks, ROV spesific coefficients are found. By choosing the material of the different components, rigid body information such as center of gravity, moment of inertia matrix and body mass is found. Then the model has been simplified by removing small appendages as nuts, bolts, engravings,

cables and holes such that the amount of vertices in the resulting model is held at a reasonable level. The sensor casings initially designed as cylinders are modified to be octagonal prisms and the manipulator arm has been removed. The resulting mesh model is shown in Figure 3.2.

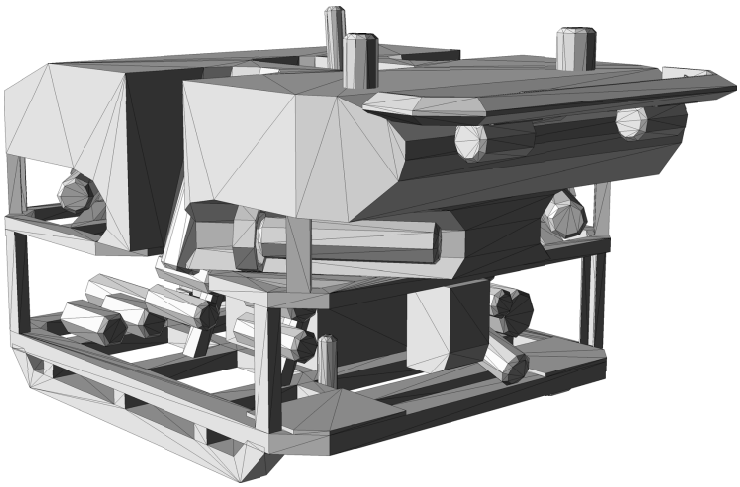

Figure 3.2: Simplified model as a rastered mesh model

The reason for simplifying the model is to reduce the number of vertices. This is done because a software package, WAMIT, has been utilized to calculate the hydrodynamic coefficients. WAMIT solves a system of equations proportional to the number of vertices, and because the model is reduced, significant improvements in computational time can be achieved by such a reduction.

To analyze a vehicle in WAMIT, the vehicle geometry has to be represented by a mesh model. This mesh models consists of a large number of small panels. One of the techniques used to calculate the coefficients are calculation of the pressure normal to each of these panels and integrating these. This results in forces and moments caused by the fluid velocity potential.

3.1 Rigid body system inertia matrix

The origin of the vehicle body frame is chosen to coincide with the center of gravity. In the body frame the rigid body mass matrix is:

$$\mathbf{M}_{RB} = \begin{bmatrix} 627 & 0 & 0 & 0 & 0 & 0 \\ 0 & 627 & 0 & 0 & 0 & 0 \\ 0 & 0 & 627 & 0 & 0 & 0 \\ 0 & 0 & 0 & 79.4 & -2.34 & 17.92 \\ 0 & 0 & 0 & -2.34 & 116.77 & -1.84 \\ 0 & 0 & 0 & 17.92 & -1.84 & 136.12 \end{bmatrix} \tag{3.1}$$

3.2 Restoring forces

The restoring forces is found by using (2.29)-(2.33), where m is found from (3.1) and ∇ and $\mathbf{r}_b^b$ are calculated by WAMIT to be:

$$\nabla = 0.604914[\mathrm{m}^3]$$
$$\mathbf{r}_b^b = \begin{bmatrix} -0.008016 \\ -0.004540 \\ -0.277778 \end{bmatrix} [\mathrm{m}]$$

Because the z-component of $\mathbf{r}_b^b$ is negative, $z_b < 0$, the vehicle is naturally stable in roll and pitch.

3.3 Coefficients from WAMIT

The coefficients for added mass, potential damping, and wave load amplitudes has been found. The results from WAMIT are output as numerical files in a non-dimensional form, and have to be made dimensional according to the user manual before use. It must be noted that the data are calculated in the stationary seakeeping frame and have to be transformed to the NED-frame. According to [Fossen and Smogeli, 2004] the data from WAMIT can be transformed into the body frame by using transformation matrices as:

$$\mathbf{M}_A(\omega) = \mathbf{T}_W \mathbf{M}_A^{WAMIT} \mathbf{T}_W^\top$$
$$\mathbf{B}(\omega) = \mathbf{T}_W \mathbf{B}^{WAMIT} \mathbf{T}_W^\top$$
$$\boldsymbol{\tau}_{hyd} = \mathbf{T}_{rao} \boldsymbol{\tau}^{WAMIT}$$

where

$$\mathbf{T}_W = \begin{bmatrix} 1 & 0 & 0 & 0 & 0 & 0 \\ 0 & -1 & 0 & 0 & 0 & 0 \\ 0 & 0 & -1 & 0 & 0 & 0 \\ 0 & 0 & 0 & 1 & 0 & 0 \\ 0 & 0 & 0 & 0 & -1 & 0 \\ 0 & 0 & 0 & 0 & 0 & -1 \end{bmatrix}$$

$$\mathbf{T}_{rao} = \begin{bmatrix} 1 & 0 & 0 & 0 & 0 & 0 \\ 0 & 1 & 0 & 0 & 0 & 0 \\ 0 & 0 & -1 & 0 & 0 & 0 \\ 0 & 0 & 0 & -1 & 0 & 0 \\ 0 & 0 & 0 & 0 & -1 & 0 \\ 0 & 0 & 0 & 0 & 0 & 1 \end{bmatrix}$$

3.3.1 Added mass and damping

In [WAMIT, 2011] the hydrodynamic coefficients are calculated based on the assumption of zero-velocity. Because the speed of ROVs are relatively low, it is assumed that these coefficients can be used directly .

The added mass (A) and damping (B) are according to the manual made non dimensional using

$$\bar{A}_{ij} = \frac{A_{ij}}{\rho L^k} \quad \text{and} \quad \bar{B}_{ij} = \frac{B_{ij}}{\rho \omega L^k} \tag{3.2}$$

where $\bar{A}_{ij}$ and $\bar{B}_{ij}$ are the non-dimensional coefficients, ρ is the water density, ω is the excitation frequency and L is the characteristic length of the vehicle. $k = 3$ for $i, j = 1, 2, 3$, $k = 4$ for $i = 1, 2, 3, j = 4, 5, 6$ or $i = 4, 5, 6, j = 1, 2, 3$ and $k = 5$ for $i, j = 4, 5, 6$. In Figure 3.3 and 3.4 the frequency dependent added mass and damping for some of the coupled degrees of freedom are shown. The red circles indicates the points where WAMIT has calculated values and the blue curve is the result of a cubic interpolation between the points.

3.4 Excitation force RAO

The excitation forces and moments from regular waves with different wave frequencies and incident wave angles has been found. WAMIT produces numerical output files containing the phase, non-dimentional amplitude, imaginary and real complex part for each combination of wave frequencies and incident wave angles. Following the manual the excitation forces (X) have been made non-dimensional using the relation in (3.3).

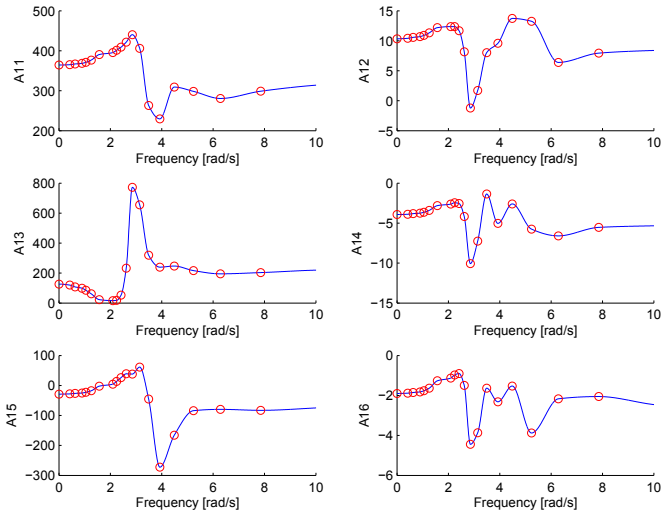

Figure 3.3: Frequency dependent added mass calculated by WAMIT in some degrees of freedom

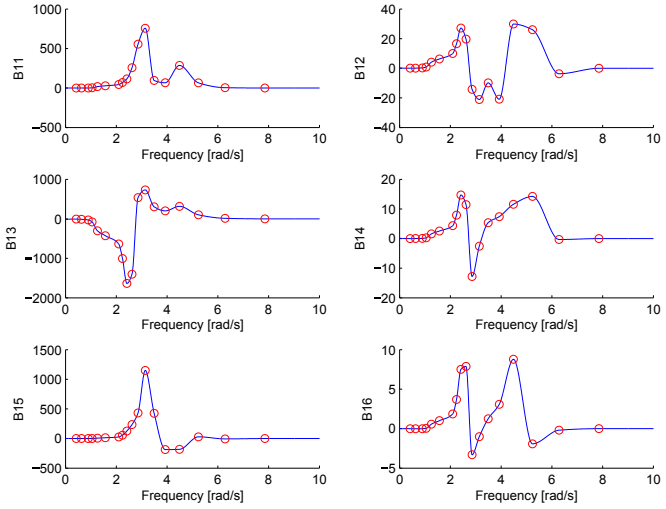

Figure 3.4: Frequency dependent potential damping calculated using WAMIT

$$\bar{X}_i = \frac{X_i}{\rho g A L^m} \tag{3.3}$$

where $\bar{X}_{ij}$ is the non-dimensional excitation force, ρ the water density, g the gravitational constant, A the wave amplitude and L is characteristic length. $m = 2$ for $i = 1, 2, 3$ and $m = 3$ for $i = 4, 5, 6$.

In Figure 3.6 and 3.5 the amplitude of the force in surge and sway is shown for different incident wave angles and frequencies is shown. Because the forces are dependent of the wave amplitude, the unit is force divided by wave amplitude. It can be seen that the force varies significantly dependent on both the angle and wave period. The maximum amplitudes of the forces in surge and sway are in the area of the buoyancy force in magnitude, and are thus assumed to be correct.

The forces on the vehicle is found by the sum of all wave components. The contribution from each wave component j in each degree of freedom is given in (3.4):

$$\tau_{env}^{WF} = \sum_{j=1}^{N} \bar{X}_{(\cdot)} \rho g A_j^2 L^{(\cdot)} \sin(\omega_j t - \epsilon_{pos} + \epsilon_j + \epsilon_{wamit_j})\sigma \tag{3.4}$$

where ω is the wave period, t is the time, j indicates the wave component, ψ_{w_j} is the angle of incident wave component j, σ is given by (2.20) and $\epsilon_{(\cdot)}$ is given by

$$\begin{aligned} \epsilon_{pos} &= \sin(\psi_{w_j})y + \cos(\psi_{w_j})xk_j \\ \epsilon_j &= \text{incident wave phase for component j} \\ \epsilon_{wamit_j} &= \text{force phase found by WAMIT for component j} \end{aligned}$$

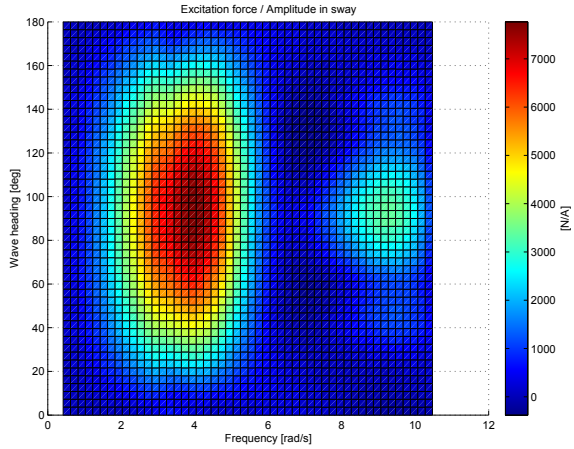

Figure 3.5: Excitation load amplitude/amp in sway for different headings and wave frequencies

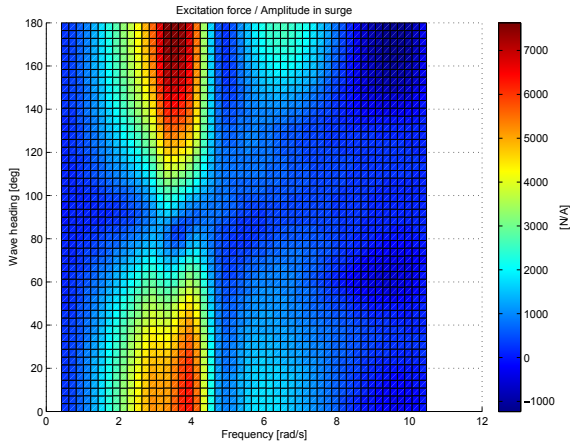

Figure 3.6: Excitation load amplitude/amp in surge for different headings and wave frequencies

3.5 Mean wave drift load

As in the case for excitation forces the numerical output for mean drift are made non-dimensional. For the case of unidirectional wave, this is done according to the relation in (3.5)

$$\bar{F}_i = \frac{F_i}{\rho g A^2 L^k} \tag{3.5}$$

where $\bar{F}_i$ is the non-dimensional force/moment and $k = 1$ for the forces ($i = 1, 2, 3$), and $k = 2$ for the moments ($i = 4, 5, 6$). The complete mean drift force is assumed to be the sum of the contribution from each wave component i. Each element in the mean drift force vector $\boldsymbol{\tau}_{env}^{MD}$ can be found by

$$\tau_{env}^{MD} = \sum_{i=1}^{N} \bar{F}_i \rho g A_i^2 L^{(\cdot)} \tag{3.6}$$

In WAMIT the calculation of the mean wave drift loads can be calculated using either a pressure integration method or a calculate it using momentum consideration. In a similar manner as for excitation loads, the result using pressure integration for surge and sway is shown in Figure 3.7(a) and 3.8(a). The corresponding result from momentum consideration is shown in Figure 3.7(b) and 3.8(b). Noticing the magnitude of the amplitude it is apparent that the calculation of mean force are incorrectand it has been concluded that the mean drift load calculations carried out can not be trusted.

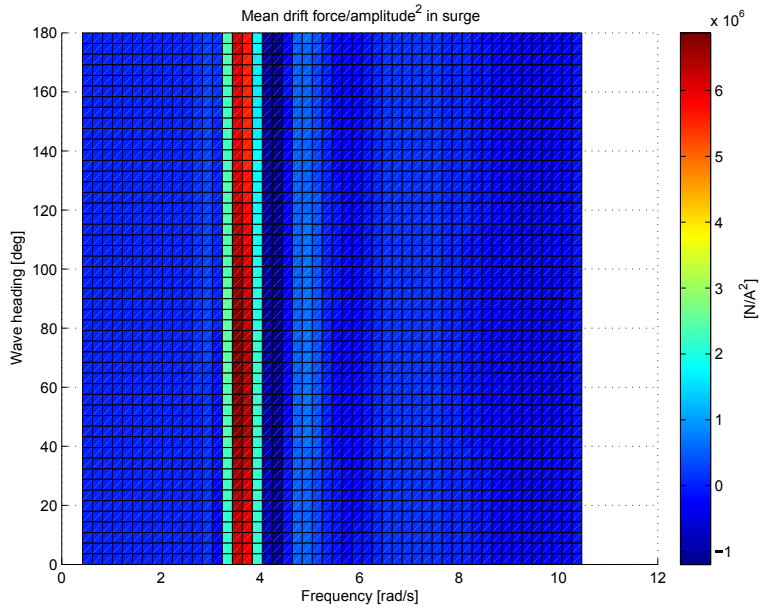

(a) Mean wave drift load amplitude/amp squared in surge for different headings and wave frequencies from pressure integration

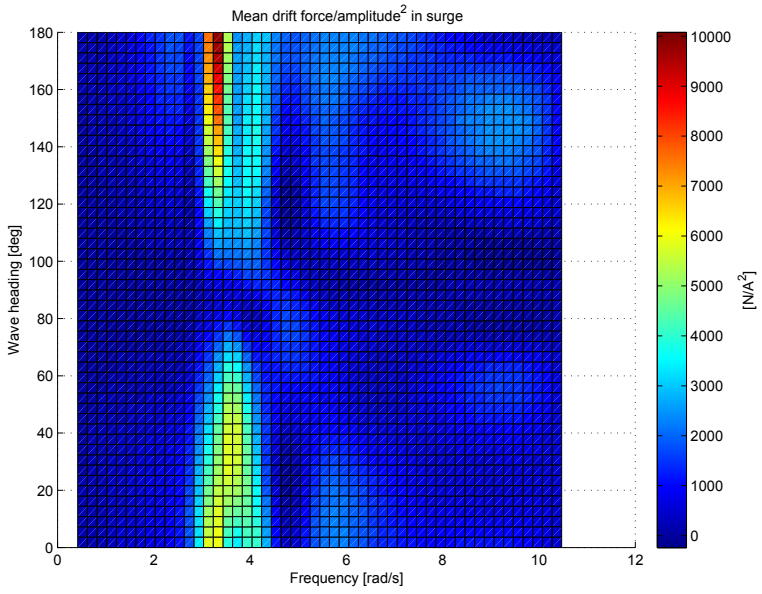

(b) Mean wave drift load amplitude/amp squared in surge for different headings and wave frequencies from momentum considerations

Figure 3.7: Mean wave drift loads comparison for surge

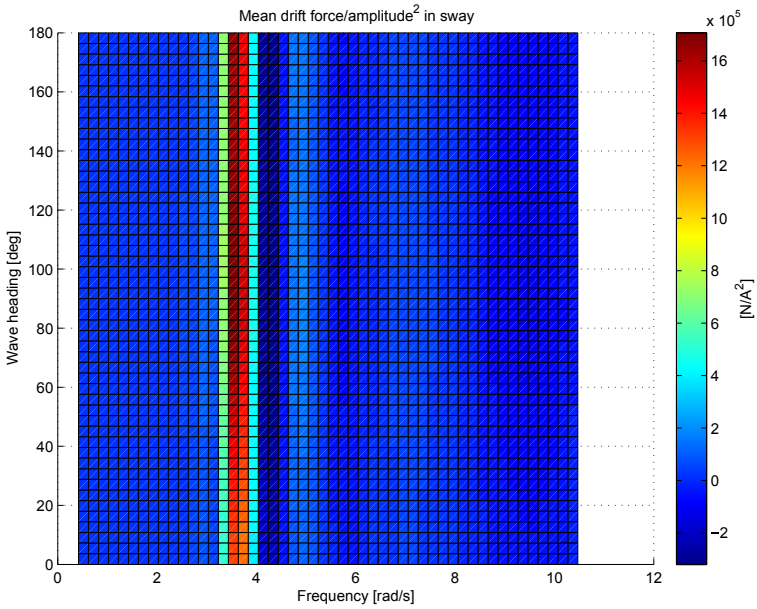

(a) Mean wave drift load amplitude/amp squared in surge for different headings and wave frequencies from pressure integration

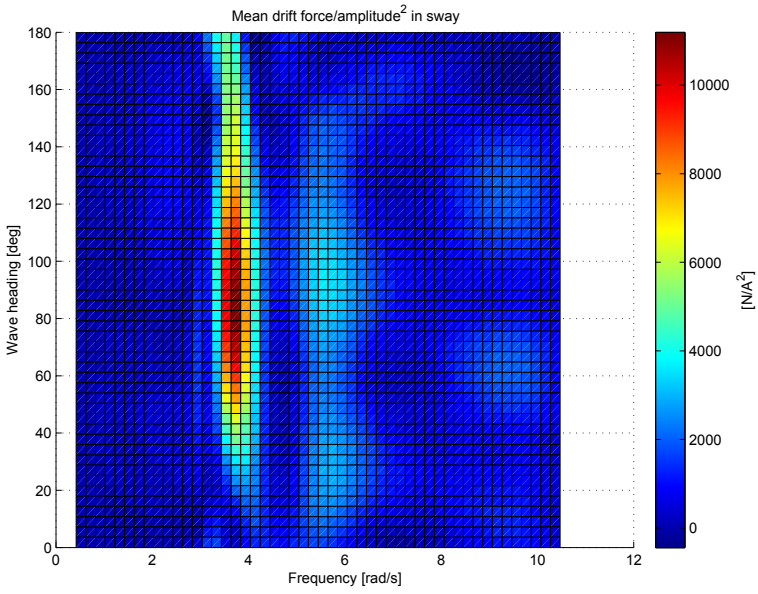

(b) Mean wave drift load amplitude/amp squared in surge for different headings and wave frequencies from momentum considerations

Figure 3.8: Mean wave drift loads comparison for sway

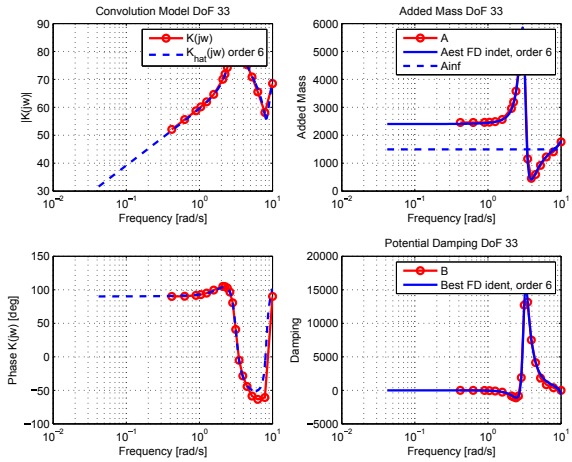

Figure 3.9: Fluid Memory transfer function for coupled 33 dofs

3.5.1 Fluid memory effects

The transfer functions for the coupled fluid memory effects are generated by the MSS FDI Toolbox based on the frequency dependent added mass and potential damping data found using WAMIT. Some of the transfer functions are plotted in Appendix B. With the use of MATLAB state space models of the different fluid memory effect contributions are calculated.

3.6 Comment on the wave loads

Based on the results for first and second order wave load amplitudes from WAMIT, it has been concluded that the wave loads can not be trusted. The wave influence on the ROV will thus in the following sections be simulated by a synthetic wave force model neglecting the fluid memory effect. Assuming infinite water depth and linear wave theory, the wave loads have been implemented as a perturbation in the position. In linear wave theory, the relation between the wave height and wave length is given as in 3.7[Faltinsen, 1990].

$$\frac{h}{\lambda} < \frac{1}{7} \tag{3.7}$$

where h is the wave height and λ is given in 4.3. Using these relations and assuming that because of its size, the ROV follow the wave, the amplitudes of the

perturbations can be expressed as

$$\eta_{wa}^1 = \frac{\lambda}{2} = \frac{\pi g}{\omega^2} \tag{3.8}$$

$$\eta_{wa}^3 = \frac{h}{2} = \frac{\pi g}{7\omega^2} \tag{3.9}$$

Thus, the perturbations in the NED frame are expressed as

$$\boldsymbol{\eta}_w^s = \mathbf{J}(\psi_w) \begin{bmatrix} \eta_{wa}^1 \\ 0 \\ \eta_{wa}^3 \\ 0 \\ 0 \\ 0 \end{bmatrix} \sin(k\sqrt{x^2+y^2} - \omega t)\sigma \tag{3.10}$$

where t is the time, ψ_w is the main wave direction, $\mathbf{J}(\psi_w)$ is the 6DOF transformation matrix between the wave frame and the NED frame and σ is the depth scaling factor described in 2.20 This results in an elliptic motion.

3.7 Hydrodynamic damping

Due to the fact that the coefficients in the damping matrices for Argus Mariner is unknown, and the shape of an ROV is not suitable for damping calculations based on strip theory, coefficients from similar vessels or scale models can be used.

In [Steen, 2007] three types of similarity is required for model tests to be good representations of the reality:

- Geometric similarity means that the model has to be geometrically similar to the full scale object. Every dimension on the model has to have the same scale among themselves as in full scale.
- Kinematic similarity means that similarity in speed is required. The ratio between different velocities has to be the same.
- Dynamic similarity deals with the relationship between different forces, e.g. inertia forces and friction forces. Similarity in Froude number F_n is typically used.

Assuming that Minerva, an ROV owned by NTNU, is a scale model of Argus Mariner, the damping coefficients can be calculated. Some of the coefficients of Minerva has been reported in [Kirkeby, 2010] and [Ludvigsen and Ødegaard, 2005]. Because the shape of Argus Mariner is different from the shape of Minerva, the geometric requirement will be violated, but as a best estimate this has still been used.

	Minerva	Argus Mariner	Ratio
Length[m]	1.44	1.575	1.09375
Height[m]	0.80	0.893	1.11625
Width[m]	0.82	1.100	1.34146

Table 3.1: Table of the scale ratios between Minerva and Argus Mariner

Using Froude-scaling the scale factor for force is given as:

$$F_f = \frac{\rho_f}{\rho_m}\lambda_s^3 F_m \tag{3.11}$$

where F_f and F_m is the force in full scale and model scale respectively, ρ_f and ρ_m is the fluid density in full scale and model and λ_s is the ratio between the characteristic design length of full scale and model vehicle, $\lambda_s = \frac{L_f}{L_m}$. The main dimensions in Argus Mariner and Minerva and their ratios are given i Table 3.1.

By choosing the scale ratio to be that of the largest length in each cross section for the different degrees of freedom, *width, length, length, width, length, length* are used for surge, sway, heave, roll, pitch and yaw respectively. This results in the following matrices for the linear and quadratic damping:

$$\mathbf{D}_L = \begin{bmatrix} 564 & 0 & 0 & 0 & 0 & 0 \\ 0 & 382 & 0 & 0 & 0 & 0 \\ 0 & 0 & 84 & 0 & 0 & 0 \\ 0 & 0 & 0 & 39 & 0 & 0 \\ 0 & 0 & 0 & 0 & 39 & 0 \\ 0 & 0 & 0 & 0 & 0 & 33 \end{bmatrix} \tag{3.12}$$

$$\mathbf{D}_{NL} = \begin{bmatrix} 705|u_r| & 0 & 0 & 0 & 0 & 0 \\ 0 & 764|v_r| & 0 & 0 & 0 & 0 \\ 0 & 0 & 830|w_r| & 0 & 0 & 0 \\ 0 & 0 & 0 & 203|p| & 0 & 0 \\ 0 & 0 & 0 & 0 & 193|q| & 0 \\ 0 & 0 & 0 & 0 & 0 & 131|r| \end{bmatrix} \tag{3.13}$$

3.8 Actuator forces

Thrusters

Argus Mariner is equipped with six fixed attitude, controllable speed thrusters which all can be controlled separately. Using the expression in (2.13) with $\delta\theta = 0$,

Thruster	x_t	y_t	z_t	θ_t	ϕ_t	D	T_i
Front port	0.457	-0.326	-0.195	-140	90	0.122	0.5
Front st.board	0.457	0.326	-0.195	140	90	0.122	0.5
Rear port	-0.580	-0.382	-0.195	140	90	0.122	0.5
Rear st.board	-0.580	0.382	-0.195	-140	90	0.122	0.5
Vertical port	0.028	-0.388	-0.274	90	160	0.122	0.5
Vertical st.board	0.028	0.388	-0.274	-90	160	0.122	0.5

Table 3.2: Description of the thruster configurations

the term $\boldsymbol{\tau}_{act}$ in (2.3) can be expressed as

$$\boldsymbol{\tau}_{thr} = \sum_{k=1}^{6} \boldsymbol{\tau}_{thr}^{k}$$

where $\boldsymbol{\tau}_{thr} \in \mathbb{R}^6$ is the combined forces and moments from all the thrusters, given in the vehicle body frame and $\boldsymbol{\tau}_{thr}^{k}$ is the forces and moments from thruster k on the vehicle in the same frame.

The propellers on the thrusters are small and light, and it is thus assumed that the response to a step in the rotational speed reference is fast, giving small time constants. All the thrusters are of the same size and type and the thrust configuration is given in Table 3.2.

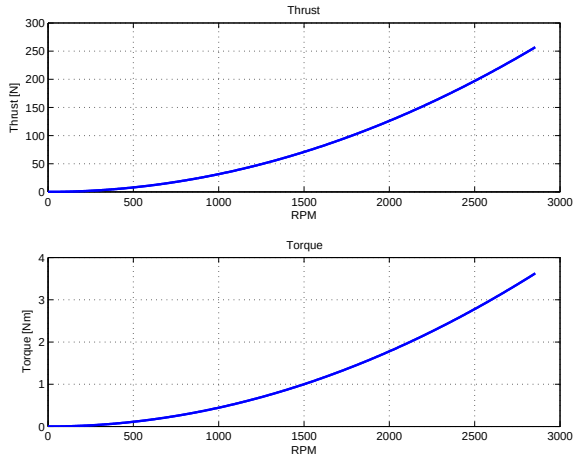

Figure 3.10: Thrust and Torque versus RPM collected from Argus Remote Systems

From the manufacturer of Argus Mariner, rpm-thrust and rpm-torque curves have been collected. These can be seen in Figure 3.10 and shows a second order relation. Because this is the only available information about the thrusters at time being, this relation between the rotational speed and thrust produced is used to model the

thrust. It must be noted that the curves only cover the first quadrant. This means that the relation is only valid when both the inflow velocity and the rotational speed are positive. The four quadrant scheme is shown in Figure 3.11. Because the propellers of this ROV are hydrodynamically optimized to positive rotations, it is assumed that the efficiency decreases in the other three quadrants. This loss is guessed to be 30%. A standard thrust loss for each individual thruster is in addition assumed to be 15% due to interaction effects.

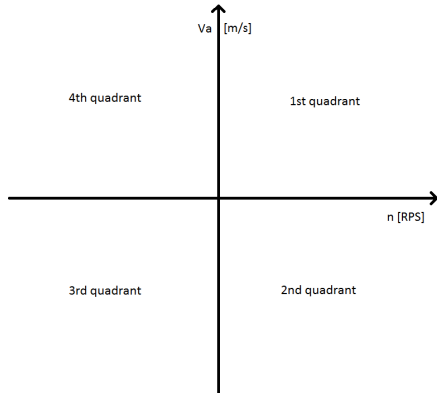

Figure 3.11: Sketch of the four quadrant scheme in thruster modelling

Chapter 4

Control System

Todays advances and inventions within consumer products are to a large extent realized using control theory. Almost everything from toys for an average 5-year old, to washing machines and cars have embedded computers or programmable logical circuits containing a control system. From the simple screaming doll which screams when sensors records a motion, to advanced collision avoidance systems in vehicles on the road. Within marine and shipping applications the early control system were autopilot systems making the ship maintaining its heading by simple mechanical means. Todays advanced control systems usually consists of a large number of electro and electromechanical components. The control system architecture of the ROV Minerva owned by NTNU is depicted in Figure 4.1.

4.1 A general marine real time control system

This architecture is an example of a local optimization control system. According to [Sørensen, 2010] and Figure 4.2 a marine control system can be divided into two main parts:

1. **Mission management** or operational management typically includes fleet management and mission planning. At this level the control is typically made manually at the headquarter.
2. **Real-time control**
    - *Local optimization* typically includes the guidance system. According to the operation, an optimization is done and appropriate reference models are used.
    - *Plant control* typically consist of observers, controllers and thrust allocation, with the purpose of controlling the vessel in accordance with the input of the guidance system.

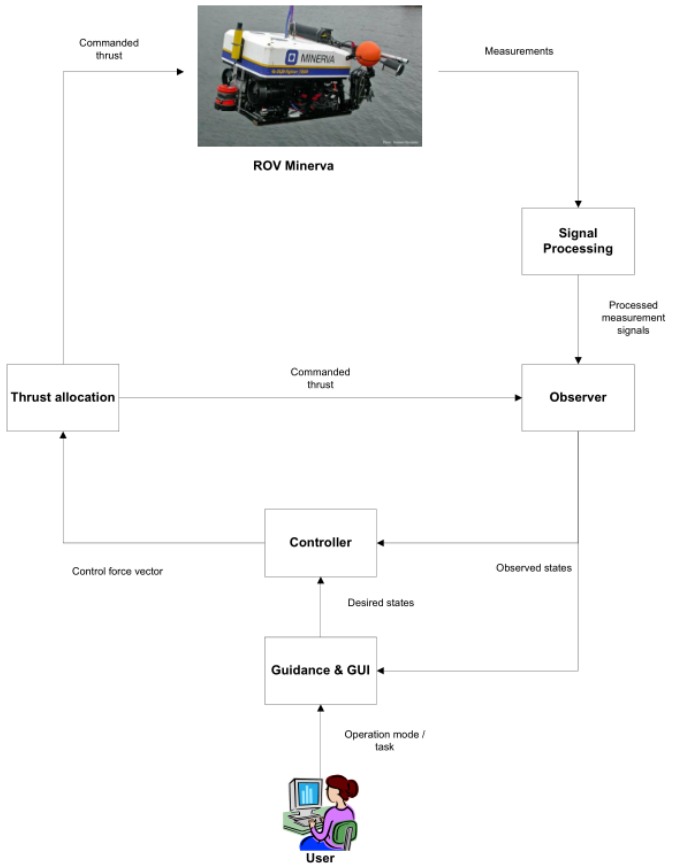

Figure 4.1: Control system architecture overview of Minerva, NTNU. Courtesy of Fredrik Dukan

- *Actuator control* is typically located locally at the actuator with the purpose of controlling the actuator in accordance with the input from the plant control system. This includes adjustment of for instance speed, pitch, torque or power. It can also include the processes required to fulfill the given commands in the case of load shedding.

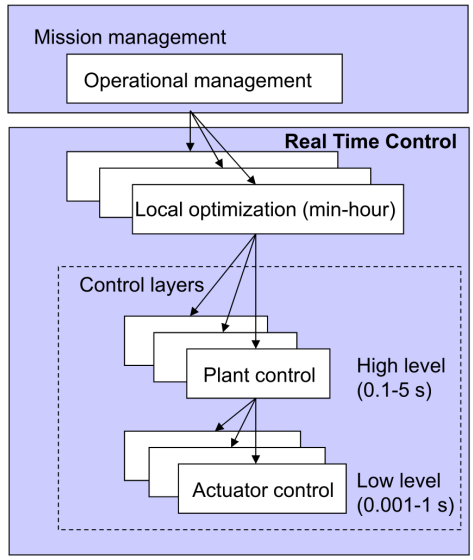

Figure 4.2: Structure of a marine control system [Sørensen, 2010]

4.2 Motion control system for Argus Mariner

4.2.1 Signal Processing

As part of a control system the sensors are very important. The sensors measures the different states such that the controllers can perform the desired actions. The signal is typically sampled from a continuous process in discrete time. This results in signals in discrete time and a ZOH-circuit is often used to convert the signal into continuous time. In many cases the same state is measured by several sensors. This results in duplicates with different values. A signal weighting and voting system can generate a combined signal such that the rest of the system receives only one signal per state. In case of sensor failure or signal freeze the signal processing system should detect this and report it to the rest of the system such that precautions against system instability and faults can be made.

4.2.2 Observer

Many vessels lack the ability to measure all states. In addition to signal and process noise this introduces the need for an observer. The observer is used to filter out sensor and process noise and to make estimates of the modelled states. For a vessel performing dynamic positioning (DP) an observer will typically filter out process and signal noise and generate position and velocity estimates. In addition, an observer will provide the ability to operate without one or more measurements, so

called *dead reckoning*. If the control system operates in dead reckoning mode, the estimates states will experience drift.

The process noise can usually be divided into a low frequency (LF) and a wave frequency (WF) part. The WF part of the noise is usually not compensated for because the noise does not matter for the particular operation or because the vessel has inadequate control capabilities available to cancel out the motions. Compensating for the WF motions caused additional wear and tear on the system.

The LF noise typically consist of slowly varying current and other unmodelled terms. Because of the LF nature of this noise it is usually handled by the motion control system. See Figure 4.3 for an illustration of low frequency and wave frequency motions.

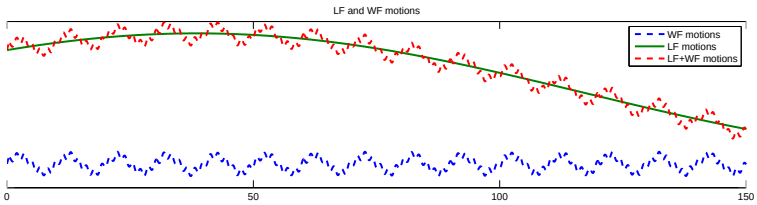

Figure 4.3: Illustration of LF and WF motions

On the ROVs currently operated by NTNU a linearized Kalman filter is used. Because only four degrees of freedom are controlled, the observer is reduced to cover only these. The heading is discretized into 19 headings with a 10 degree steps, where each heading has its own tuning matrix. Because of the linearisation, the observer has only so much accuracy. An extended Kalman filter is another option, but because the system becomes computationally heavy, this option is omitted. A nonlinear passive observer is chosen because of its simplicity and computational demand.

Because availability of signals for all states is assumed and no sensors are modelled, the signal to the observer are the contaminated signals. The signal processing component of the system is thus dropped.

Control plant model

The Control Plant Model (CPM) is a simplified version of the Process Plant Model (PPM) developed in Chapter 2. By neglecting terms of the PPM with small contributions, the CPM is made less computational demanding. It can then be the basis for an observer or for controller feed forward.

Nonlinear Passive Observer

As the ROV will operate in a waves and receive sampled signal with noise, it will experience both process and signal noise. By using a passive nonlinear observer the process and signal noise can be filtered out. For ships performing DP, the capability to turn off the wave filtering is desirable if the motions caused by the waves can be counteracted by the control system. The same applies for an ROV. Small waves with little impact should be ignored, while waves that can be counteracted should be counteracted. In [Sørensen, 2010] the equations for a nonlinear passive observer for a dynamic positioning (DP) surface vessel in 3DOF is given as:

$$\dot{\hat{\boldsymbol{\xi}}} = \mathbf{A}_w \hat{\boldsymbol{\xi}} + \mathbf{K}_1 \tilde{\mathbf{y}} \tag{4.1a}$$

$$\dot{\hat{\boldsymbol{\eta}}} = \mathbf{R}(\psi_y)\hat{\boldsymbol{\nu}} + \mathbf{K}_2 \tilde{\mathbf{y}} \tag{4.1b}$$

$$\dot{\hat{\mathbf{b}}} = -\mathbf{T}_b^{-1}\hat{\mathbf{b}} + \mathbf{K}_3 \tilde{\mathbf{y}} \tag{4.1c}$$

$$\mathbf{M}\dot{\hat{\boldsymbol{\nu}}} = -\mathbf{D}\hat{\boldsymbol{\nu}} - \mathbf{R}^\top(\psi_y)\mathbf{G}\hat{\boldsymbol{\eta}} + \mathbf{R}^\top(\psi_y)\hat{\mathbf{b}} + \boldsymbol{\tau}_{act} + \mathbf{R}^\top(\psi_y)\mathbf{K}_4\tilde{\mathbf{y}} \tag{4.1d}$$

$$\tilde{\mathbf{y}} = \hat{\boldsymbol{\eta}} + \mathbf{C}_w \hat{\boldsymbol{\xi}} \tag{4.1e}$$

where $\hat{\mathbf{y}}$ is the estimated position, $\tilde{\mathbf{y}} = \mathbf{y} - \hat{\mathbf{y}}$ is the error in estimated position, $\mathbf{K}_{(\cdot)}$ are observer gain matrices to be determined, $\mathbf{A}_w$ is the wave system matrix, $\hat{\boldsymbol{\xi}}$ is the wave state vector, $\mathbf{C}_w$ is the wave measurements matrix, $\hat{\mathbf{b}}$ is the bias estimate, $\boldsymbol{T}_b$ is the bias time constants, $\mathbf{D}$ is the damping matrix, $\mathbf{G}$ is the restoring matrix, $\boldsymbol{\tau}_{act}$ is the actuator vector and $\hat{\boldsymbol{\eta}}$ is the position and attitude estimate.

Because we want a 6DOF observer, the rotation matrix is changed such that $\mathbf{R}(\psi_y) = \mathbf{J}(\boldsymbol{\Theta}_y)$ and $\mathbf{R}^\top(\psi_y) = \mathbf{J}^{-1}(\boldsymbol{\Theta}_y)$. The restoring term $\mathbf{R}^\top(\psi_y)\mathbf{G}\hat{\boldsymbol{\eta}}$ is neglected because we have no external restoring forces linear to the position. The elements in (4.1a)-(4.1e) have thus the following dimensions: $\hat{\boldsymbol{\xi}} \in \mathbb{R}^{12}, \mathbf{A}_w \in \mathbb{R}^{12\times12}, \mathbf{K}_1 \in \mathbb{R}^{6\times12}, \mathbf{K}_2 \in \mathbb{R}^{6\times6}, \mathbf{K}_3 \in \mathbb{R}^{6\times6}, \mathbf{K}_4 \in \mathbb{R}^{6\times6}, \tilde{\boldsymbol{y}} \in \mathbb{R}^6, \hat{\boldsymbol{\eta}} \in \mathbb{R}^6, \hat{\boldsymbol{\nu}} \in \mathbb{R}^6, \hat{\mathbf{b}} \in \mathbb{R}^6, \mathbf{T}_b \in \mathbb{R}^{6\times6}, \mathbf{M} \in \mathbb{R}^{6\times6}, \mathbf{D} \in \mathbb{R}^{6\times6}, \boldsymbol{\tau}_{act} \in \mathbb{R}^6$ and $\mathbf{C}_w \in \mathbb{R}^{12\times6}$

Depth dependence

Because the adaptive approach assumes constant environmental parameters the depth dependence has to be dealt with by using the same approach as in (2.20) where the wave forces can be scaled according to the depth. In the case of the observer, the WF contribution to the position and attitude is scaled by the depth depending term. Assuming that the observer receives filtered sea depth measurements and that the dominating wave period is found, the equation for the complete estimated position (4.1e) can be rewritten as:

$$\hat{\mathbf{y}} = \hat{\boldsymbol{\eta}} + \sigma \mathbf{I}_{6\times6}\mathbf{C}_w\hat{\boldsymbol{\xi}} = \hat{\boldsymbol{\eta}} + \hat{\boldsymbol{\eta}}_{WF} \tag{4.2}$$

σ depends on the wave number which again depends on the wavelength. By using the connection between the waveperiod and wavelength found in [Faltinsen, 1990]

given by

$$\lambda = \frac{g}{2\pi} T^2 \tag{4.3}$$

Then the wavenumber can be found by

$$k = \frac{2\pi}{\lambda} \tag{4.4}$$

4.2.3 Guidance system

The guidance system generates a reference for the vessel to follow. This can be a way point generator with a simple third order filter based reference model or more advanced path models optimized according to weather and environment. When using simple reference generators a filter of the reference is needed so that large steps in the reference is smoothed out. Without this reference model large steps in reference cause large state-errors which can lead to an unstable system.

The goal of the guidance system in this thesis is to generate a trajectory such that the ROV follows the net cage at a small distance. Because the ROV is supposed to carry a cleaning device and inspect the cage at a later stage, it is also desired that the vehicle always has a heading close to the normal of the net. The guidance system is based on trajectory tracking, where the trajectory is generated using the assumed knowledge of the position of the nodes of the net. By using the net cage

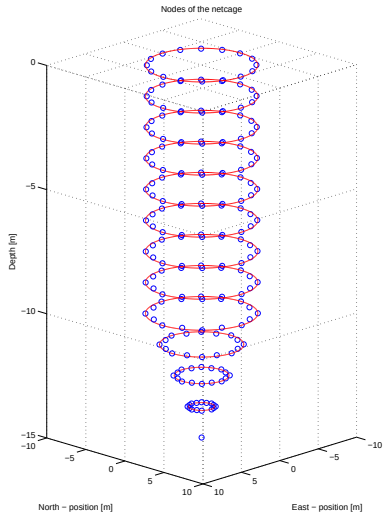

Figure 4.4: The nodes of the netcage immediately after the system startup marked as blue circles

model developed by SINTEF Fishery and Aquaculture and assuming that it is an

observer estimating the states of the net cage, the position of the different nodes can be found. These nodes are used as way points. A *way point management system* and a third order reference generator as described in [Fossen, 2011] generates a smooth trajectory.

Immediately after the start of the system the nodes are sorted such that their neighboring nodes are found. Depending on the desired route, the way point management system switches between the nodes, and a filter smoothens out the change in setpoint.

The route is generated by starting at the top going in circles each level at a time. From the current node the next one is chosen to be the neighboring node to the left or right. When all nodes on a level are visited, a node on the level below are chosen and the the process repeats itself. The trajectory ends at the bottom.

Reference model

The third order filter is given as

$$\boldsymbol{\eta}_d^{(3)} + (2\boldsymbol{\Delta} + \mathbf{I})\boldsymbol{\Omega}\ddot{\boldsymbol{\eta}}_d + (2\boldsymbol{\Delta} + \mathbf{I})\boldsymbol{\Omega}^2\dot{\boldsymbol{\eta}}_d + \boldsymbol{\Omega}^3\boldsymbol{\eta}_d = \boldsymbol{\Omega}^3\mathbf{r}^n \tag{4.5}$$

where $\boldsymbol{\eta}_d$ is the desired position and attitude, $\boldsymbol{\Delta}$ is a reference damping matrix and $\boldsymbol{\Omega}$ is a tuning matrix deciding the rate of change of $\boldsymbol{\eta}_d$.

Using fixed values in the tuning matrix $\boldsymbol{\Omega}$ may cause the system to become unstable. This will happen if $\dot{\boldsymbol{\eta}}_d$ is larger than the velocity the ROV is capable of having at the specific moment. In this case the error in the controller will increase, and if the error gets large enough it will make the system unstable. To avoid this it is possible to introduce a saturating element in the filter such that $|\dot{\boldsymbol{\eta}}_d| < \boldsymbol{\nu}_{\max}$. Another possibility is according to [Fossen, 2011] to add a nonlinear damping term to (4.5).

In this thesis the first possibility mentioned is used, saturating the velocities using the values in (4.6). These values are based on the maximum velocities of Minerva given in [Kirkeby, 2010]. By using the same scaling method as in Section 3.7 velocity can be scaled as $V_f = V_m\sqrt{\lambda}$ where subscript f and m indicates full scale and model scale respectively. The characteristic lengths are chosen to be the same as for viscous damping.

$$\boldsymbol{\nu}_{\max}^{Minerva} = \begin{bmatrix} 1.03 \\ 0.5 \\ 0.5 \\ 1.05 \end{bmatrix} \Rightarrow \boldsymbol{\nu}_{\max}^{Argus} = \begin{bmatrix} 1.03\sqrt{1.34} \\ 0.5\sqrt{1.09} \\ 0.5\sqrt{1.09} \\ 1.05\sqrt{1.09} \end{bmatrix} = \begin{bmatrix} 1.19 \\ 0.52 \\ 0.52 \\ 1.10 \end{bmatrix} \tag{4.6}$$

Assuming $\boldsymbol{\eta}_d$ is critically damped gives us the reference damping matrix:

$$\boldsymbol{\Delta} = \mathbf{I} \tag{4.7}$$

4.2.4 Controller

By calculating the difference between the desired and estimated state, the controller typically calculates the forces and moments needed to minimize the error. These desired forces and moments are the sent to the control allocation.

The controller implemented in this thesis is a nonlinear PID controller based on the one in [Fossen, 2011]. It is chosen because of its simple structure and because it can be easily tuned. The control law is chosen as

$$\boldsymbol{\tau}_{PID} = -\mathbf{J}^{\top}(\boldsymbol{\Theta})[\mathbf{K}_p\tilde{\boldsymbol{\eta}} + \mathbf{K}_d\mathbf{J}(\boldsymbol{\Theta})\tilde{\boldsymbol{\nu}} + \mathbf{K}_i\int_0^T \tilde{\boldsymbol{\eta}}\mathrm{d}t] \tag{4.8}$$

where $\mathbf{K}_p$, $\mathbf{K}_i$, $\mathbf{K}_d$ are the tuning matrices for the proportional, integral and derivative term respectively, and $\tilde{\boldsymbol{\eta}} = \boldsymbol{\eta} - \boldsymbol{\eta}_d$ In addition a reference feedforward term using a reference model as described in [Sørensen, 2010] is added:

$$\boldsymbol{\tau}_{FF} = \mathbf{M}\mathbf{a}_d + \mathbf{D}_L\boldsymbol{\nu}_d + \mathbf{D}_{NL}(\boldsymbol{\nu}_d) \tag{4.9}$$

where $\mathbf{M} = \mathbf{M}_{RB} + \mathbf{M}_A(\infty)$ are the rigid body mass and added mass, $\mathbf{D}_L$ is the linear damping and $\mathbf{D}_{NL}(\boldsymbol{\nu}_d)$ the quadratic damping.

The complete control force is thus given as

$$\boldsymbol{\tau}_{thr} = \boldsymbol{\tau}_{PID} + \boldsymbol{\tau}_{FF} \tag{4.10}$$

Integral wind-up

Combining an integral action with an actuator that can saturate, can as earlier mentioned lead to undesired effects. If a large error persists over time the integral gets very large. When the error eventually decreases the integral is still large, causing the integral term of the controller to dominate the controller output. Because it can take a long time for the integral to decrease it is desirable to introduce an anti-windup term limiting the integral part of the output. This is done in two stages. This is done by stopping to integrate when the error-integral gets larger than a predefined value. Then the integral term is altered to the value found by (4.11).

$$\boldsymbol{\tau}_i = \mathbf{K}_i\int\tilde{\boldsymbol{\eta}} + \mathbf{K}_{anti}[\mathrm{sat}(\mathbf{K}_i\int\tilde{\boldsymbol{\eta}}, \boldsymbol{\tau}_{min}, \boldsymbol{\tau}_{min}) - \mathbf{K}_i\int\tilde{\boldsymbol{\eta}}] \tag{4.11}$$

where $\boldsymbol{K}_{anti}$ is the matrix of anti windup tuning constants and $\mathrm{sat}(\mathbf{K}_i\int\tilde{\boldsymbol{\eta}}, \boldsymbol{\tau}_{min}, \boldsymbol{\tau}_{min})$ calculates the saturated value of the force.

4.2.5 Control allocation

The control allocation uses the output from the controller and the knowledge of the actuator configuration to determine the individual control signal to each actuator. The expression in (2.10) can be utilized to calculate the load on the drive. Using the relation between torque and rotational speed of the propeller, the ability to use a torque controller as an alternative to a traditional speed controller for thruster control is added. This has not been conducted in this thesis.

In the case of the Argus Mariner ROV the control actuators consist of fixed attitude, controllable speed propellers. The control input to each thruster is assumed to be a signal representing the desired revolutions per minute(RPM). All the motors and propellers on the ROV are of the same type. In [Sørensen, 2010] the thrust allocation can be done using the following equation:

$$\boldsymbol{\tau}_c = \mathbf{T}_{con}\mathbf{K}\mathbf{u} \tag{4.12}$$

$$\Rightarrow \mathbf{u} = \mathbf{K}^{-1}\mathbf{T}_{con}^{\dagger}\boldsymbol{\tau}_c \tag{4.13}$$

where $\boldsymbol{\tau}_c$ is the commanded thrust, $\mathbf{T}_{con}$ is the thruster configuration matrix, $\mathbf{T}_{con}^{\dagger}$ is its pseudo inverse, $\mathbf{K}$ is a diagonal matrix of thrust force coefficients and $\mathbf{u}$ is the thruster control input vector.

Using the information about the thruster configuration in Table 3.2 and Figure 3.10 the elements of $\mathbf{T}_{con}$ and $\mathbf{K}$ can be found. The relation between rpm and thrust is quadratic and the control input vector is given as:

$$\mathbf{u} = |\mathbf{n}|\mathbf{n} \tag{4.14}$$

where $\mathbf{n}$ is the vector of RPM input to the different thrusters. The desired rpm is thus found from

$$\mathbf{n} = \text{sign}(\mathbf{u})\sqrt{|\mathbf{u}|} \tag{4.15}$$

4.2.6 Signal modelling

Due to the small time-step of the integrators of the model, $\boldsymbol{\eta}$ and $\boldsymbol{\nu}$ are assumed to be continuous. In addition they are smooth. If it is assumed that we have measurements of all states in $\boldsymbol{\eta}$ and $\boldsymbol{\nu}$, the simulated states can be fed directly to the control system. Using these values directly as sensor signals is unrealistic. Real signals are contaminated by noise and the states are sampled at a given frequency. To simulate this condition, the signal of each state is assumed to be sampled from the following continuous signal:

$$x_n = x_{st}\zeta_n w_n \tag{4.16}$$

where x_n is the continuous signal with noise, x_{st} is the state, ζ_n is the noise amplitude and w_n zero mean Gaussian white noise. Using a Zero order hold (ZOH) approach the continuous-time measurement signal is as shown in Figure 4.5.

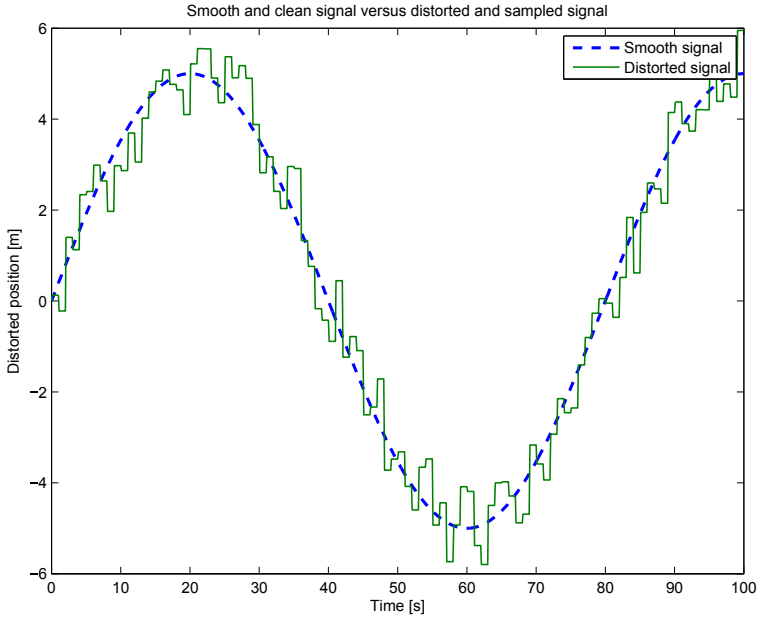

Figure 4.5: Sampled signal with added noise

Chapter 5

Simulation environment

The process plant and control system has been implemented in a simulation environment named FhSim . It has been developed by SINTEF Fishery and Aquaculture AS to be an aid in product development. The ability to visualize the results is added to simplify debugging and to enable SINTEF to show their customers simulations of products and proposed solutions. It is also proposed to be used for simulator training within certain areas in the future. It is well equipped to handle systems modelled as Ordinary Differential Equations (ODE) and contains a database of models and tools that can be used in various projects.

FhSim is written in the Object Oriented Programming (OOP) language C++, and the models developed in this thesis have thus been implemented following an object oriented structure.

5.1 Object Oriented Programming

In Wikipedia a good review of OOP is found. is considered to be a paradigm within computer programming and the concept origins from work done in the 1960s. By separating to program code into *classes*, where each class has its own limited area of responsibility, the classes can be reused by other programs. The use of a class is done by create one or more *instances* of the class. These instances are called *objects*. To accomplish reusability of the code most OOP languages supports three main principles:

- Encapsulation
- Inheritance
- Polymorphism

5.1.1 Encapsulation

Each object encapsulates some data, *variables*, and some functionality,*methods*. By providing an interface, other objects are able to make the object perform different tasks by calling the methods defined in the interface. Both the variables and the methods are common to all instances of the class, but the values of the variables belongs to the instantiated object itself.

5.1.2 Inheritance

Inheritance allows to create classes that inherits data and functionality from other classes and even extend them with extra data and functionality.

5.1.3 Polymorphism

Polymorphism offers the possibility of an object to act as another object. As long as the interface of the acting object satisfies the interface of the object it mimics, this is possible.

5.2 Classes

When planning to build a system within an OOP-framework it is recommended to start by planning how the system is going to be interconnected, and how the relationship between the different classes are supposed to be. Simobjects, short for simulation objects, are in FhSim the super class of all objects to be simulated. FhSim has already implemented several SimObjects such as environment with waves, current and bottom topography, a dynamic net cage model and a cable model. These are all classes inheriting the class 'SimObject' and extends its functionality by adding class-specific data members and methods.

Other more specialized cases of a marine craft such as a ROV, extends the behaviour of a general vessel. To illustrate the resemblance between similar types of objects and the relations between them, a class diagram as shown in Figure 5.2 can be drawn. The class diagram shows inheritance as arrows, both UUVs and Surface vessels are of type Marine Vessel, and relations as a single line. From the relation link it can be seen that one marine vessel can have several forces, and a force belongs to one vessel.

5.2.1 Process plant model

A process plant model is a high fidelity model describing the main contributions to a system. Figure 5.2 shows a class diagram of the proposed PPM and how each class

inherits another. The 'SimObject' class contains methods and variables necessary to communicate with the main program. As seen, the class 'PotentialVessel' inherits the 'SimObject' class. Inside the 'PotentialVessel' class vessel specific variables concerning the added mass, potential damping and rigid body characteristics such as center of buoyancy, mass matrix, volume and so on are stored. This is done to increase the reusability.

In this thesis WAMIT is used to calculate the potential properties, but another alternative, ShipX Veres developed by MARINTEK can also be used. The data from Veres is not output in the same way as WAMIT and needs a different method to read the data from file, even though it contains mostly the same data. Using the 'PotentialVessel' class, both a 'WamitVessel' and a 'VeresVessel' can inherit from it. Then the read method implemented in the child class can assign values to the correct variables in the parent class. This also make the code easier to change, because a change only has to be performed one place.

The non potential forces and moments such as viscous forces and moments also have to be included, and it is decided that this is to be included at the 'WamitVessel' level.

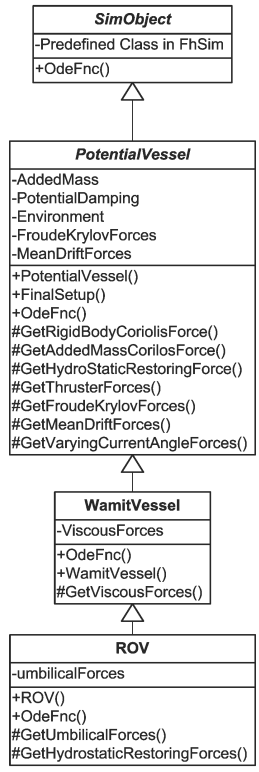

Figure 5.1: Succession of inheritance for the ROV class

If we compare a general surface vessel with an ROV it is apparent that an ROV has additional forces and moments. One example is the forces and moments due to the umbilical. The hydrostatic restoring forces and moments are also different, because the submerged volume will decrease when the ROV is at the surface. The result of this is that the first three elements in the restoring vector becomes zero.

In Figure 5.1 the succession of inheritance for the ROV class in shown. This figure shows the main variables and the methods. As can be seen all classes have the method 'OdeFnc'. This method calculates the values to be integrated by the state integrator. Because 'OdeFnc' is dependent on some ODEs it is not implemented in the 'SimObject' class itself, but instructs the inheriting classes to implement it. This is an example of the previously mentioned polymorphism.

When the main program tell all the Simobjects to run the method 'OdeFnc' the ROV object calls methods in the parenting classes. For instance, since the ROV object does not have a method implementing the calculation of the rigid body Coriolis and centripetal force, the ROV tries to find it in its parent. Since the method is not implemented in this class either, it tries the parent of the parent, namely the 'PotentialVessel'. Then, this method is called and the ROV continues to the next statement in its OdeFnc.

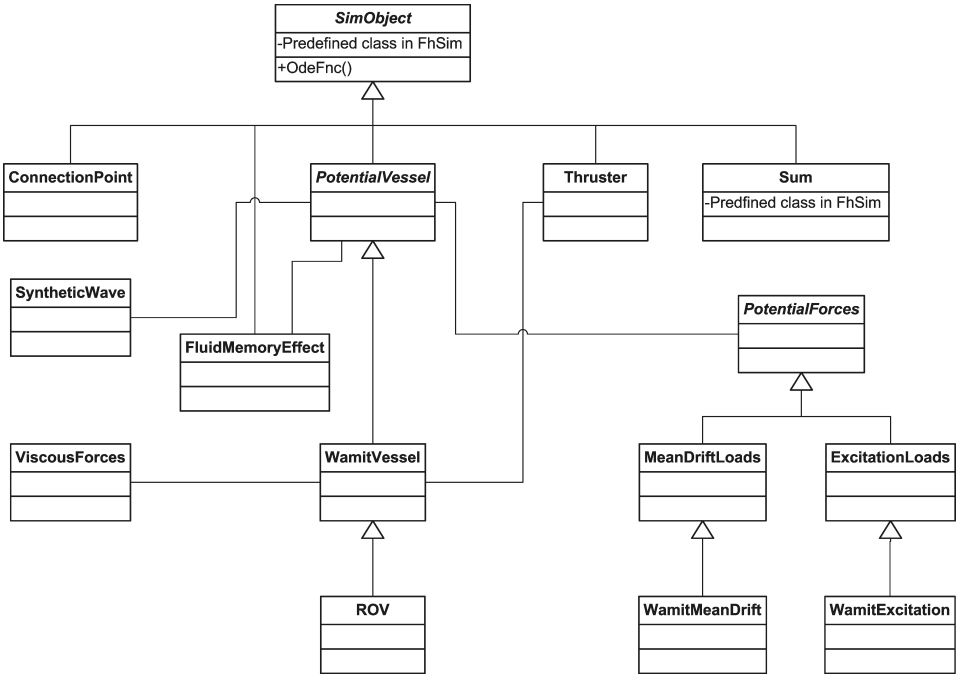

Figure 5.2: Class diagram of the process plant model

As can be seen from the diagram in Figure 5.2, some classes are not inheriting from the 'SimObject' class. This is because they do not have any internal states

themselves, and thus inheriting from 'SimOject' is not necessary. In the case of 'ViscousForces' class, it only needs the velocity to the vessel to calculate the forces. The wave load classes inheriting from 'WaveForcesWAMIT' only have to know the position of the vessel in addition to information about the waves.

The class 'WamitVessel' and the children of 'PotentialForce' class all implements methods for automatically reading the output files from WAMIT. This includes the rigid body matrix, volume, center of buoyancy and the hydrodynamic coefficients, such that the only vehicle specific coefficients to be defined in the setup file are the linear and quadratic damping matrices, and the vessel main dimensions.

The fluid memory effect has in this thesis been implemented as separate fluid memory elements. Every fluid memory element is its own 'SimObject', where the coefficients for the state space model have to be defined in the setup file.

5.2.2 Control system

As in the case of the process plant model, a class diagram of the control system is also recommended to draw before starting to write code. To make the control system as general as possible to increase the reusability, the class diagram in Figure 5.3 has been made.

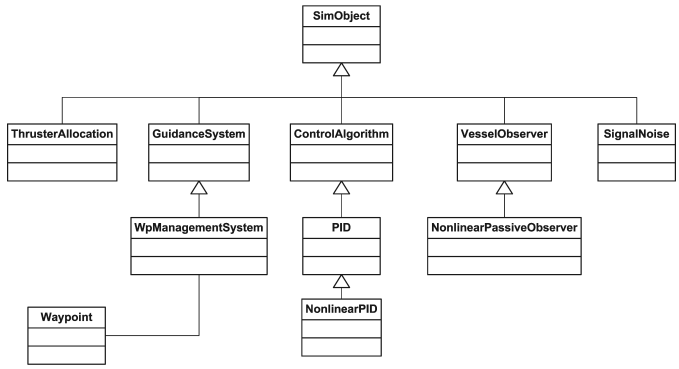

Figure 5.3: Class diagram of the control system

Observer

A general parent class called 'VesselObserver' has been proposed. This parent defines the main input and output of an observer. A child of the 'VesselObserver' class called 'NonlinearPassiveObserver' is also proposed.

Control Algorithm

The general controller class 'ControlAlgorithm' defines the standard input and output of a controller, where the child class 'PIDController' is a specialized class. The class 'NonlinearPID' inherits the 'PIDController' class.

Control Allocation

The control allocation is implemented as a simple thruster allocation with fixed thrusters. By reading input from the setup file, the 'ThrusterAllocation' simobject generates the thruster configuration and coefficient matrices.

The ability to input coefficients for both a linear and second order relation between the rpm and thrust are implemented. By using the quadratic relation, the thruster allocation will more accurately calculate the rpm input vector to the thrusters, leading to increased response to large steps in $\boldsymbol{\tau}_c$. For a thruster with large time constant, the accuracy in thrust allocation will in general not increase the response. Thus, depending on the available thruster data, either A_{thr}^{quad} and B_{thr}^{quad} or B_{thr}^{lin} are to be given. If only the linear coefficient B_{thr}^{lin} is given as input in the setup file, the quadratic relation is calculated as

$$A_{thr}^{quad} = \frac{B_{thr}^{lin} n_{max}}{n_{max}^2} \tag{5.1}$$

$$B_{thr}^{quad} = 0 \tag{5.2}$$

To get more accurate thrust input to the observer the commanded thruster forces and moments from each thruster i are recalculated using the following equations:

$$\tau_{thr}^{i} = \text{sign}(n_i)[A_{thr}^{quad} n_i^2 + B_{thr}^{quad} |n_i|] \tag{5.3}$$

Guidance System

The guidance system in this thesis is as earlier described a third order filter with velocity saturation and a way point management system. The way point managements system implements the ability to predefine way points using the setup file in addition to the automatic generation based on the netcage nodes.

The netcage traverser option start by first sorting the nodes in the netcage. First by depth using a *bucket sort* algorithm and then by north position using a *quicksort* algorithm. The bucket sort algorithm is described in Algorithm 1. According to [Cormen et al., 2001] the bucket sort algorithm has linear run time if the elements that to be sorted are uniformly distributed over the interval and the number of buckets are sufficiently large. At worst this sorting algorithm has cost n^2 where n is the number of elements to be sorted. The quicksort described in Algorithm 2 is a recursive algorithm with a best cost of $n \log(n)$. At worst it has a cost of n^2. The

cost is highly dependent on the choice of pivot element. Because the n-position of the nodes can be considered bounded, the pivot element is chosen to be the one in the middle of the list.

Algorithm 1 Pseudocode of implemented bucket sort algorithm

```
1: Create a bucket for each integer of the depth
2: for all nodes do
3:     Calculate the integer of the node-depth
4:     Put node into the bucket corresponding to the integer depth
5: end for
6: for all nonempty buckets do
7:     Sort using another algorithm
8: end for
9: Concatenate the content of all buckets together in order.
```

Algorithm 2 Pseudocode of implemented quick sort algorithm

```
1: Choose a pivot node
2: Create a list for smaller and a list for larger nodes than the pivot
3: for all nodes do
4:     if node >= pivot then
5:         insert node into larger
6:     else
7:         insert node into smaller
8:     end if
9: end for
10: call quickSort on smaller
11: call quickSort on larger
12: Concatenate the content from smaller to larger
```

After the elements are sorted, the neighboring nodes of each node at each level in the cage are found. When all nodes on one level have both a left and a right neighbor, the next level is processed. The algorithm for finding the neighbors is described in Algorithm 3 below.

Algorithm 3 Pseudocode of implemented neighbor-node-finding algorithm

```
1: for all quick sorted buckets do
2:     for all nodes do
3:         Using node_i, find the two closest nodes
4:         Set the neighbor relations of the three nodes
5:     end for
6: end for
```

Chapter 6

Simulations

The PPM and control system briefly described in Chapter 5 has been implemented in FhSim and simulated using the output from WAMIT found in Chapter 3. As mentioned, the wave frequency forces have been neglected, and a synthetic wave model driving a perturbation in position has been used instead.

6.1 Effect of current on the ROV

In FhSim the water column are divided into layers, each with its own current speed and heading. By giving a flag to the controller telling it to only control the depth and neglect the other degrees of freedom, the effect of ocean current can be observed. In Figure 6.1 the distorted measurement signal of the position together with the estimated position shows that the observer is able to filter out the signal noise and create a position estimate with little distortion. Because the current velocity is rather small in this case, the signal with noise becomes very chaotic.

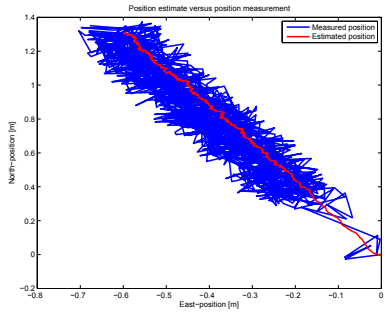

Figure 6.1: Position estimate of the ROV exposed to current

6.2 The effect of the thruster dynamics

As the implementation of the thrusters are general and dependent of the coefficients given at time of initialization, the effect of thruster dynamics can be shown by choosing a large time constant. In Figure 6.2 the result for a thruster with the time constant $T_i = 15$ is shown. It can be seen that the steps in rpm is smoothed out. For an ROV the thruster dynamics are considered negligible because of the small time constants.

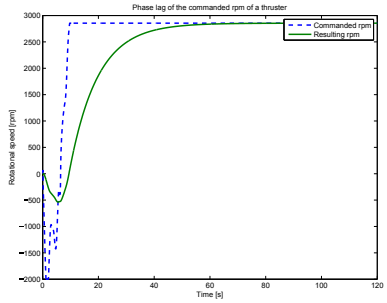

Figure 6.2: Effect of the thruster dynamics.

6.3 Waypoint tracking

As the ROV is supposed to traverse the net of a fish cage that is moving continuously, a guidance system has been implemented to provide tracking capabilities. In

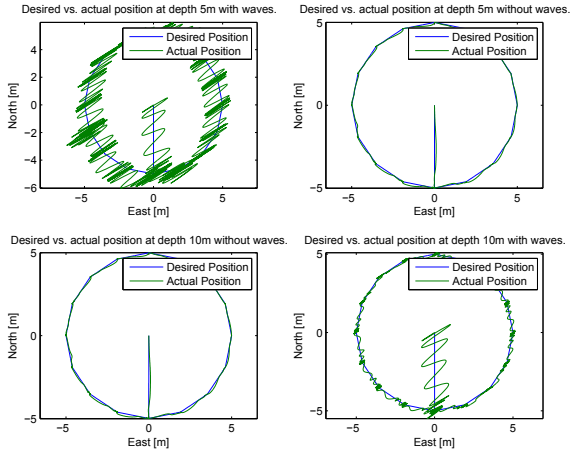

Figure 6.3: The effect of waves over depth.

Figure 6.3 the result of tracking nodes that are stationary, with and without waves in two different depths, are shown. The direction of the main wave component can clearly be seen. Starting in the middle of the circle, the ROV heads for the first way point. Because of the natural frequency in all DOFs are given when initializing the reference model, the force in surge saturates when the ROV tries to follow the reference. This occupies the thrusters such that limited thrust is available in sway to control the error. This can be seen in the Figure 6.4, where the saturation can be observed in the beginning. When the ROV reaches the first way point, the thrusters are again capable of controlling multiple directions. The top left plot in Figure 6.3 shows that the vehicle is unable to counteract the wave motions at lower depths.

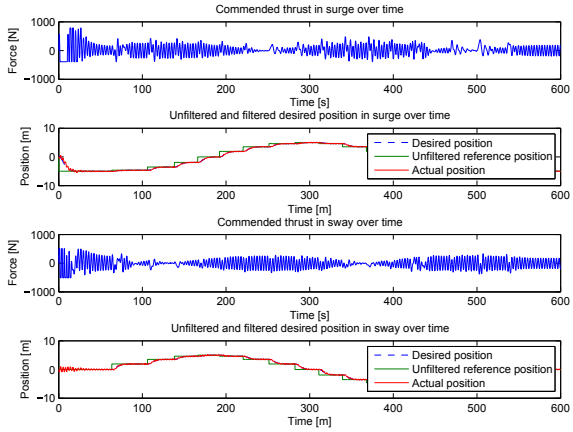

Figure 6.4: The effect of waves over depth.

6.4 DP in waves

The effect of the depth term of the waves can also be seen during dynamic positioning if the desired down-position changes. In Figure 6.5 the depth dependence is easily seen. As the ROV starts at a depth of five meters, it gets a new position reference of three meter. Already at five meters the influence of waves is noticed, but increases when the depth decreases. After reaching the desired depth, it descends to 10 meters and the influence of waves almost vanishes.

6.5 Automatic traversing of dynamic waypoints

In Figure 6.6 a result of a partial simulation of the use of the automatic WP generation algorithm. The top circle is traversed nicely, while it in the second one

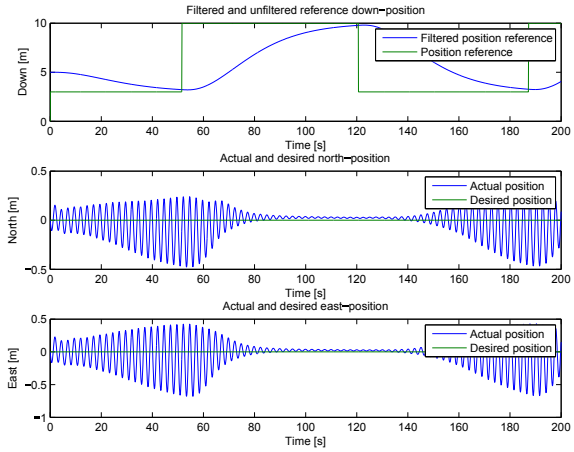

Figure 6.5: The effect of waves over depth.

can be observed an error. It struggles to find a way point, but traverses further after finding it. On the third level it seems as the algorithm crashed giving only two separate node points. The node points are marked with red circles and the blue line is the actual path traversed.

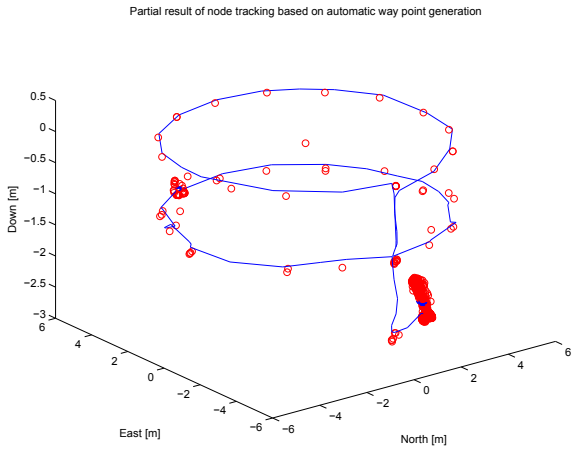

Figure 6.6: Result of automatic WP generation and tracking based on net cage model

Chapter 7

Discussion

The main focus in this thesis has been the modelling of an ROV in the wave zone. As most ROVs used today are operated beneath the wave zone, little work have been reported on the interaction between small and complex bodies and the waves. As the ROV is small compared to the wave length, it has been assumed that the ROV follow the wave particles in an elliptic pattern. To further investigate if this is the case, full scale experiments should be done.

7.1 WAMIT results

Several problems using the software for wave interaction analysis have been encountered. Because the calculated added mass and damping have the same order of magnitude as the vehicle mass and buoyancy forces, they are assumed to be a good approximation of the actual values. The simplification by eliminating the manipulator influences the result, but because it is movable, separate analysis is recommended to be conducted on the manipulator alone. The excitation wave forces and moments found are at most about ten times the maximum force produced by the thrusters.This indicates that in the case of a sea states with main wave frequency of about 4 rad/s, the vehicle is unable to counteract the wave forces near surface. The mean drift loads found have been rejected. There is no physical explanation for the drift loads having an order of magnitude of 10^6N compared to 10^3N for excitation loads. The drift loads for a tanker using WAMIT results accompanying MSS FDI Toolbox are for comparison in order of magnitude of 10^5N.

The mean loads found, leads to think that the discretized mesh model might be too complex or too simple. After a discussion with Professor Thor I. Fossen at NTNU, it has been experienced before that WAMIT is unable to calculate wave forces for some shapes. In the manual of WAMIT, it is written that the wave

loads in the vicinity of thin bodies might be inaccurate. To prevent this, another software capable of defining the thin objects in another way may be used, but as this software has not been available for the author, this solution has not been tested.

An alternative to using the given model would have been to start by representing the ROV as a box, and step step increasing the complexity. Then the wave load results from WAMIT would have been more accurate, at the expense of less accurate volume, CB, added mass and damping calculations.

In the software code developed, the ability to disable the different contributions to the complete wave force have not been added, such that results not involving the mean drift has been unavailable.

7.2 ROV CAD model

Based on the assumptions made about the materials of the different components the complete mass, center of gravity and moment of inertia tensor have been calculated. The natural stability in roll and pitch is largely influenced by the distance between the center of buoyancy and center of gravity. By assuming other materials, the center of gravity will change and the possibility of a less stable system is increased.

It must be noted by the author that the thruster configuration is found rather unpractical. Because of the shape of the propellers, they will generate most thrust at positive rotations. In the current setup, the thrusters will cause the maximum force to be larger backwards than forward. As the camera and manipulator are mounted in the front, it is assumed that the desired main direction of motion is forward, and it is thus assumed to be beneficial to have most thrust forward. In addition, it is proposed that the ROV should carry a cleaning device. These are usually based on water jets, and assuming that the device is mounted in the front, flushing water into the net, a relatively large thrust is produced. This force will be in the same direction as the thrust on positive rotations, not compensating each other, giving the ROV large problems holding its position.

7.3 The resulting mathematical model

The resulting mathematical model implemented, includes terms that are not of importance for an ROV. One of these terms are the Coriolis and centripetal force. Because of the low speed an ROV typically operates with, the contribution will be negligible compared to other terms. The reason for still including this term, is to increase the usability of the code. In the same way, the term using the relative acceleration is also included. This force will be negligible for large vessels because of the small angular velocities. Another example of such a term is the thruster

dynamics. This can be neglected for small propellers, but can have a significant impact for larger propellers.

The hydrodynamic damping included are simplified using the assumption of linear theory, where different contributions can be added together. As earlier mentioned, the damping for ROVs and AUVs are influenced by the oscillations of the vehicle (KC-number). By assuming that the ROV follows the wave particles, the contribution from oscillating inflow velocity is neglected.

7.4 Control system

The behaviour of a marine vehicle is dependent of the control system and the tuning of it. By implementing an observer, unmeasured states can be estimated, and measurements filtered. The tuning of the observer was performed, but the velocity estimates was not found to be accurate. Because the states of the system can be read directly without any noise and it is desired that the system do not filter out the wave component of the position, the results from the ROV was used directly as input to the controller.

The guidance system generates a route for the ROV in a satisfying way. As shown, the smooth desired value is highly dependent of the natural frequencies in the filter, and a method for automatically calculate these frequencies for each step in reference would increase the stability. As the guidance is only based on a simple filter, a method for decreasing the rate of change of the desired value if the ROV is unable to follow would enhance the system. There has also been shown that as the position measurement and step in the desired position has different sign, the path generated is the longest possible. Starting at for instance -179degrees going to 179degrees, the desired turn generated is 358degrees instead of -2degrees.

Chapter 8

Conclusion and further work

8.1 Conclusion

The main focus of this thesis has been the development of a process plant model for the Argus Mariner ROV for use in the wave zone. Because many of the forces and moments contributing to the model dynamics are the same for different types of vehicles, the model has been implemented in FhSim by using an ROV specialization of a general marine vessel. Using the object oriented architecture provided, several SimObject model have been implemented. By implementing the models using inheritance between similar objects, the reusability of the system developed is high, and only small modifications have to be done to simulate other marine vessel.

The implementation were highly dependent of correct results of WAMIT, and as the results were found to contain errors the main focus of this thesis, namely simulating the ROV with high frequency wave loads, a compromise by using a synthetic wave model has been made. This excludes the effect of fluid memory and the reliability of the simulations is thus reduced.

8.2 Recommendations and further work

During the work of this thesis, several new ideas have come to mind. This includes both improvements and extensions to the models and control system algorithms implemented.

8.2.1 Argus Mariner

Full scale sea-trial of the ROV should be performed to clarify if the thruster configuration is optimal. The effect of the thrusters can be improved by moving the motors of the thrusters inside the floating element, out of the propeller wake. It must also be investigated if the thruster forces available is sufficient in real life.

8.2.2 Model of Argus Mariner

The effect of KC-number and oscillating inflow on the damping should be investigated for the ROV in waves. Even though it has been shown that the damping of the motions of an ROV is dependent of the oscillating current, the ROV is still a small body in waves, and it will follow the fluid particles to an extent.

Local inflow velocities on the different body members have not been taken into account. Descriptive studies on viscous damping, thruster dynamics and thrust-reduction-effects is recommended to be performed. This will increase the accuracy of the model.

For finding potential coefficients, a new model of the ROV can be analyzed in WAMIT to investigate if the error found is due to the discretized mesh or a problem itself. An alternative can be to use other software packages to find the same coefficients.

8.2.3 Control system

Based on the results from WAMIT it can be seen that the effect of the waves on the ROV will be highly dependent of the direction of the incoming waves. By introducing a guidance system that take the main wave heading and current heading into account, the performance in position control will be increased and power consumption can be minimized.

The issue with the desired heading in the guidance system should fixed and automatic calculations of filter gains should be implemented if a filterbased reference model is to be used.

The thesis is based on the assumptions that the position of both the ROV and nodes in the net are perfectly known. In reality this is not the case.In addition, the relative position between the net and the ROV is not known. The possibility of adding a mechanism to the nodes that clearly can be detected using a ROV mounted sonar of echo sounder should be investigated. By using several cameras and image processing the relative position to the net, could also be found.

The observer implemented are dependent of input on the sea states and motion amplitudes and must be tuned individually to the current sea state. Using sea trials and experiments this data can be found, such that supervisory switching

by an operator can keep the accuracy of the observer at a desirable level. An alternative to this is to implement an adaptive observer estimating these values online.

Bibliography

[Berg, 2007] Berg, T. E. (2007). *Marine Operations - Submarines, AUVs - UUVs and ROVs*. Department of Marine Technology, NTNU.

[Cormen et al., 2001] Cormen, T., Leiserson, C., Riverst, R., and Stein, C. (2001). *Introduction to Algorithms, 2nd edition*. The Massachusetts Institute of Technology.

[Cummins, 1962] Cummins, W. (1962). The impulse response function and ship motions. Technical report, DTIC Document.

[Faltinsen, 1990] Faltinsen, O. (1990). *Sea loads on ships and offshore structures*. Cambridge University Press, Cambridge ; New York.

[Fossen, 2011] Fossen, T. (2011). *Handbook of Marine Craft Hydrodynamics and Motion Control*. Wiley.

[Fossen and Fjellstad, 1995] Fossen, T. and Fjellstad, O. (1995). Nonlinear modelling of marine vehicles in 6 degrees of freedom. *Journal of Mathematical Modelling of Systems*, 1(1).

[Fossen and Smogeli, 2004] Fossen, T. and Smogeli, Ø. (2004). Nonlinear time-domain strip theory formulation for low-speed manoeuvering and station-keeping. *Modeling, identification and control*, 25(4):201–221.

[Fossen and Perez, 2011] Fossen, T. I. and Perez, T. (2011). Marine systems simulator (mss). `www.marinecontrol.org`.

[Kirkeby, 2010] Kirkeby, M. (2010). Comparison of Controllers for Dynamic Positioning and Tracking of ROV Minerva. Master's thesis, Norwegian University of Science and Technology, Norway.

[Ludvigsen and Ødegaard, 2005] Ludvigsen, M. and Ødegaard, y. T. (2005). Fullskala thrust-test av minerva. Technical report, NTNU.

[Newman, 1977] Newman, J. (1977). *Marine hydrodynamics*. The MIT press.

[Nortrade, 2009] Nortrade (2009). Norway's vibrant seafood economy. `www.nortrade.com`.

[Ogilvie, 1964] Ogilvie, T. (1964). Recent progress toward the understanding and prediction of ship motions. In *5th Symposium on naval hydrodynamics*, pages 3–80. Bergen, Norway.

[Refsnes, 2007] Refsnes, J. (2007). *Nonlinear Model-Based Control of Slender Body AUVs*. PhD thesis, NTNU.

[SNAME, 1950] SNAME, S. (1950). *Nomenclature for treating the motion of a submerged body through a fluid: report of the American Towing Tank Conference*. Technical and research bulletin. American Towing Tank Conference.

[Sørensen, 2010] Sørensen, A. (2010). *Marine Control Systems, Propulsion and Motion Control of Ships and Ocean Structures*. Department of Marine Technology, NTNU UK-2011-76.

[Steen, 2007] Steen, S. (2007). *Marin teknikk 3 - Hydrodynamikk. Motstand og Propulsjon. Propell og foilteori*. Department of Marine Technology, NTNU UK-2007-99.

[WAMIT, 2011] WAMIT, I. (2011). Wamit user manual, version 6.4pc. `www.wamit.com`.

Appendix A

Plots of WAMIT data

The frequency dependent added mass and damping are plotted using a MATLAB script. The red circles represents the discrete points used for WAMIT evaluation. The blue line is the interpolated curve representing the continuous relation between frequency and added mass or damping.

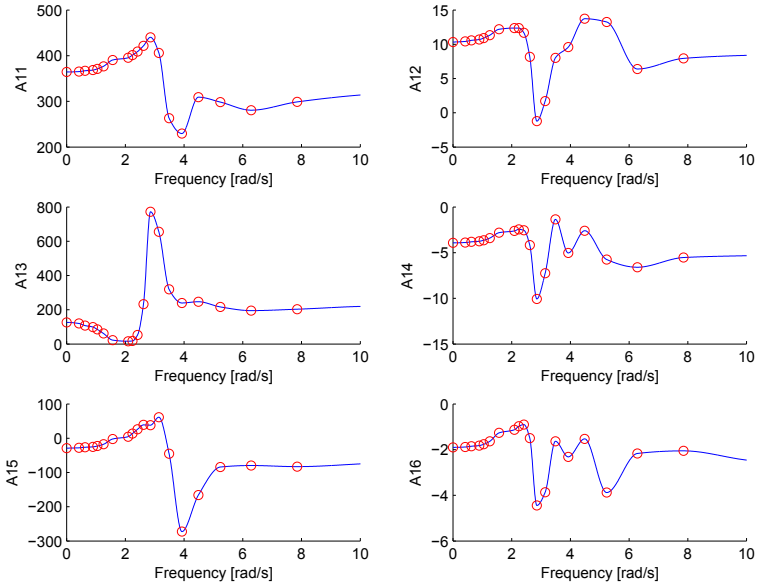

Figure A.1: Frequency dependent added mass row 1

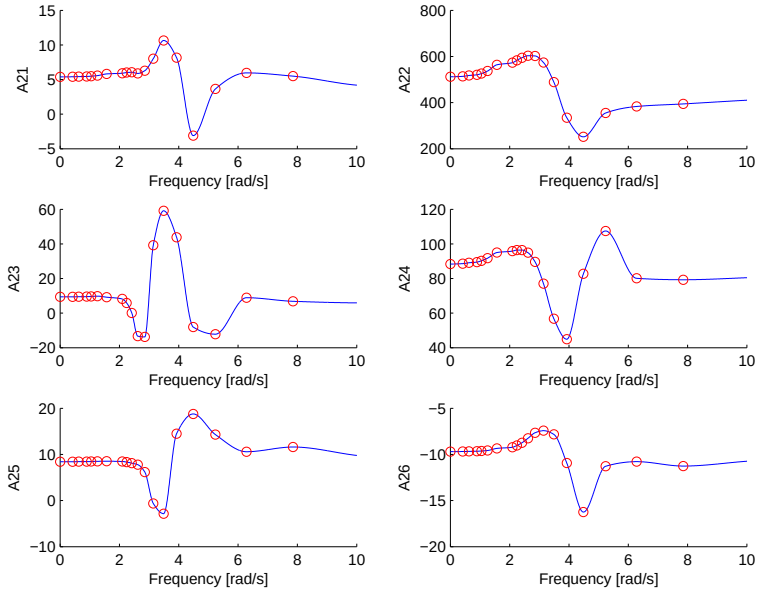

Figure A.2: Frequency dependent added mass row 2

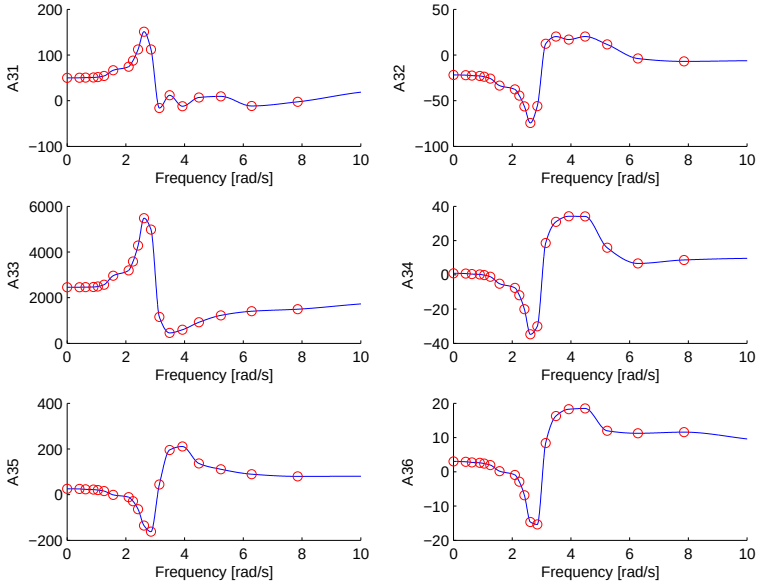

Figure A.3: Frequency dependent added mass row 3

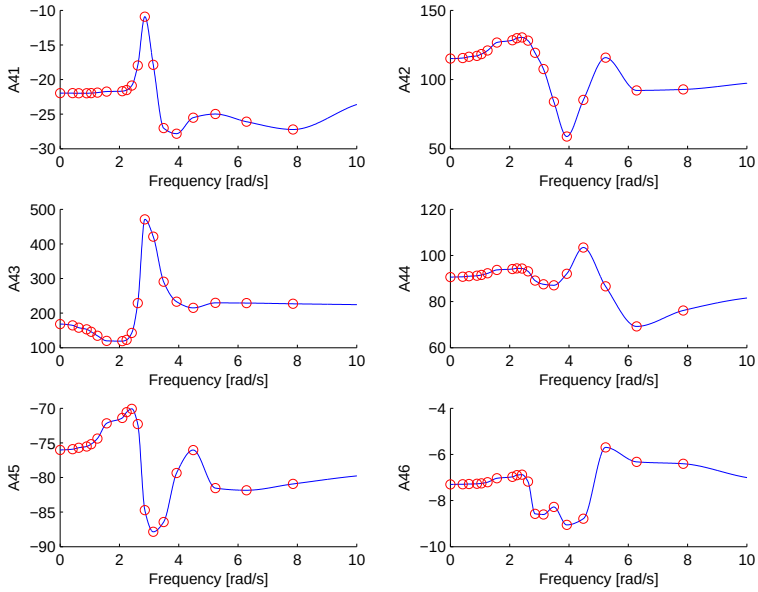

Figure A.4: Frequency dependent added mass row 4

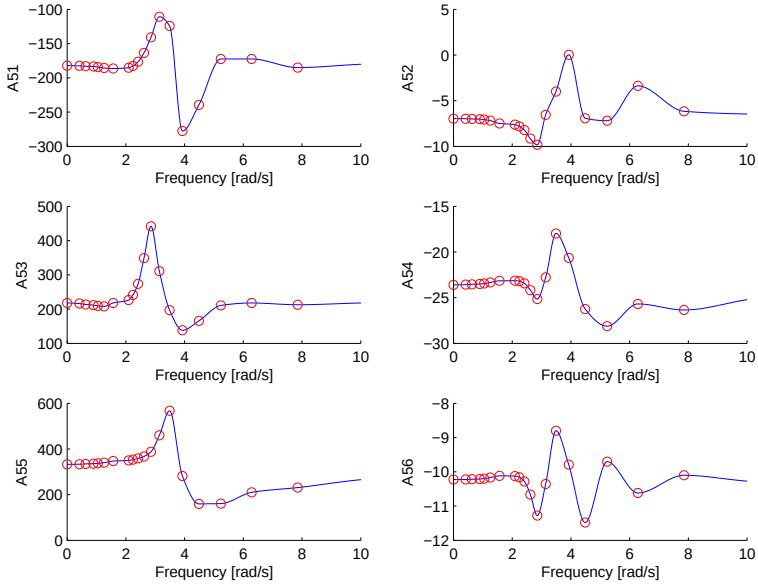

Figure A.5: Frequency dependent added mass row 5

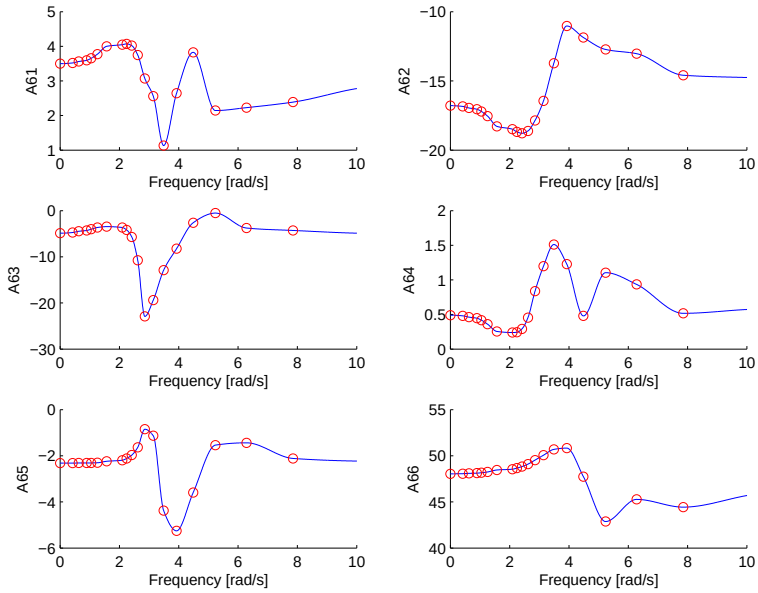

Figure A.6: Frequency dependent added mass row 6

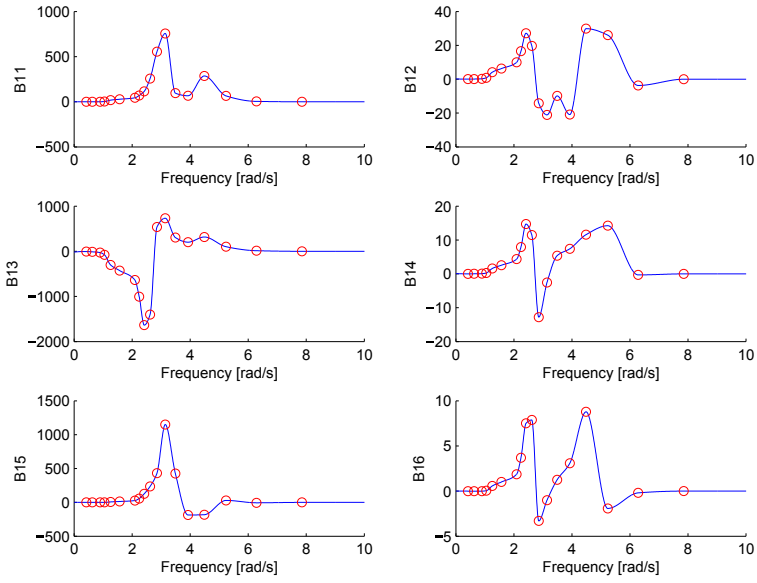

Figure A.7: Frequency dependent potential damping row 1

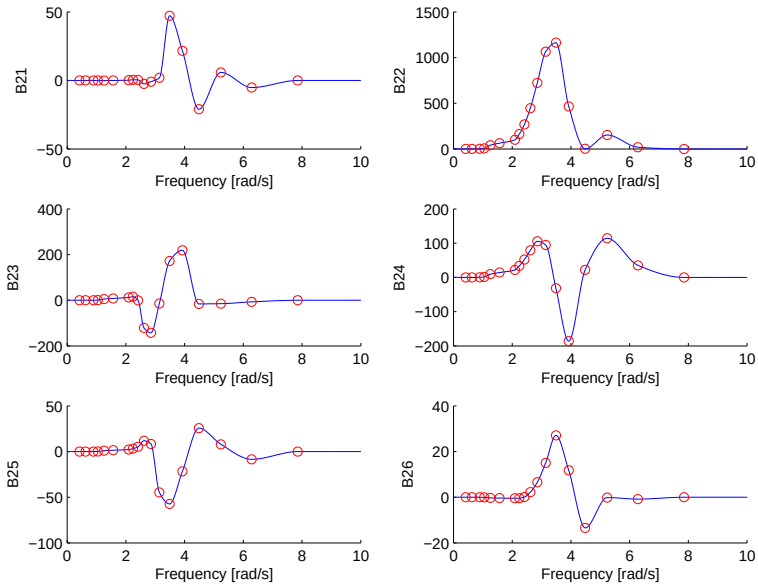

Figure A.8: Frequency dependent potential damping row 2

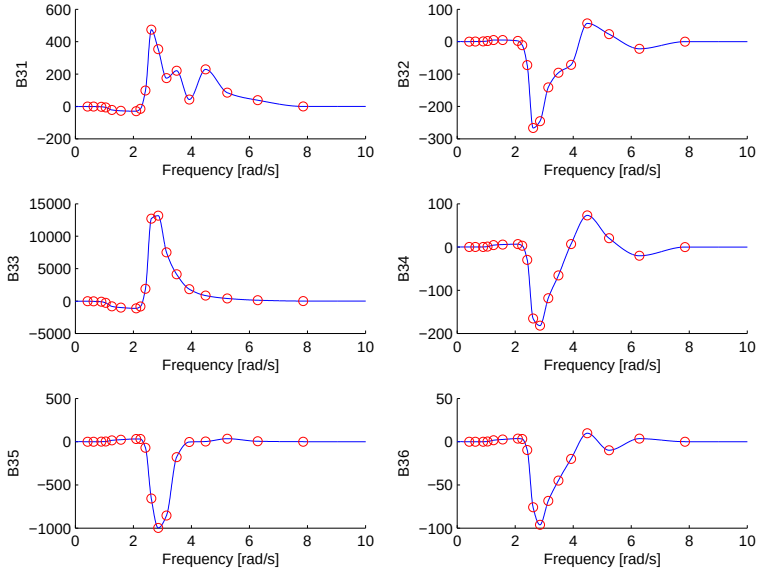

Figure A.9: Frequency dependent potential damping row 3

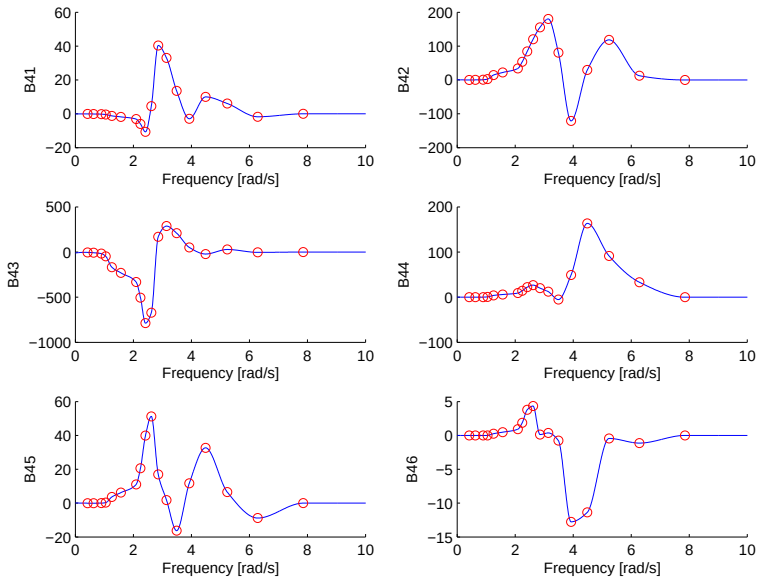

Figure A.10: Frequency dependent potential damping row 4

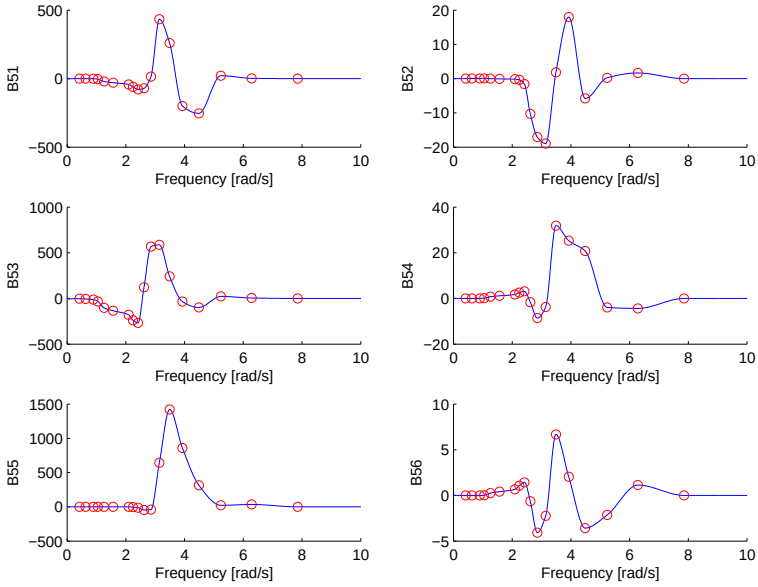

Figure A.11: Frequency dependent potential damping row 5

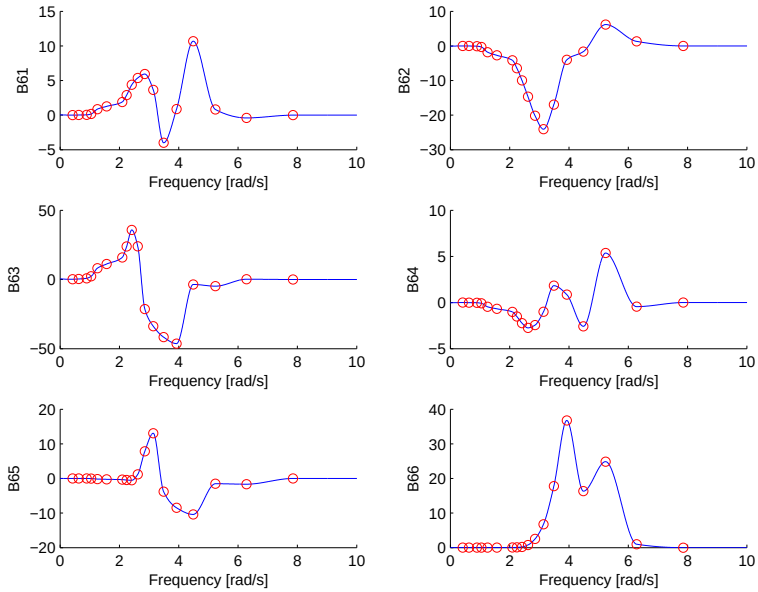

Figure A.12: Frequency dependent potential damping row 6

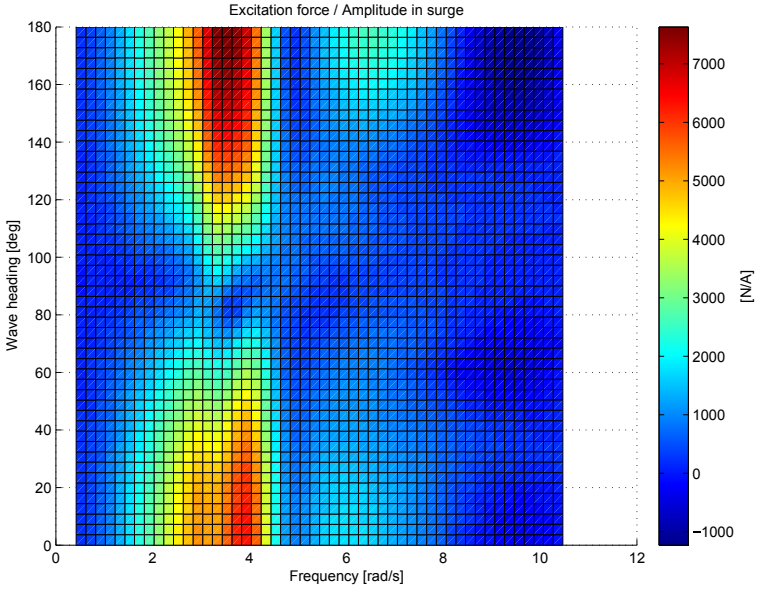

Figure A.13: Excitation load amplitude in surge for different headings and wave frequencies

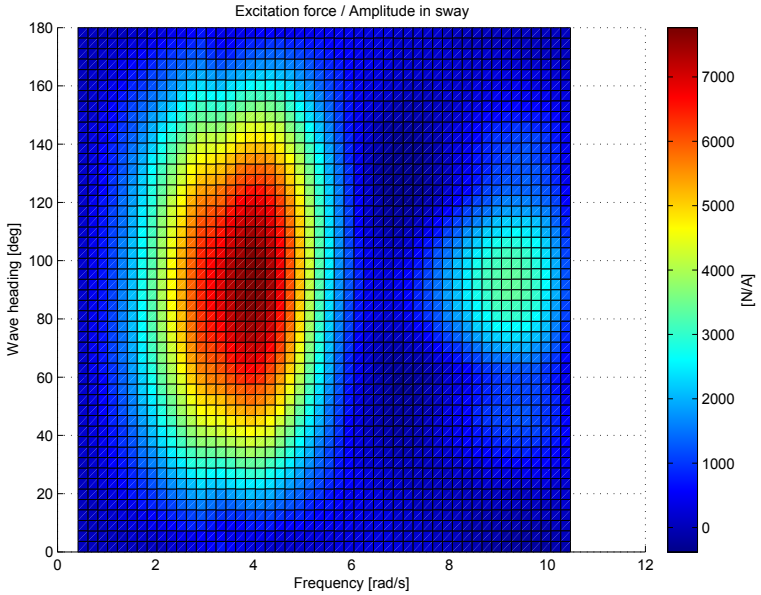

Figure A.14: Excitation load amplitude in sway for different headings and wave frequencies

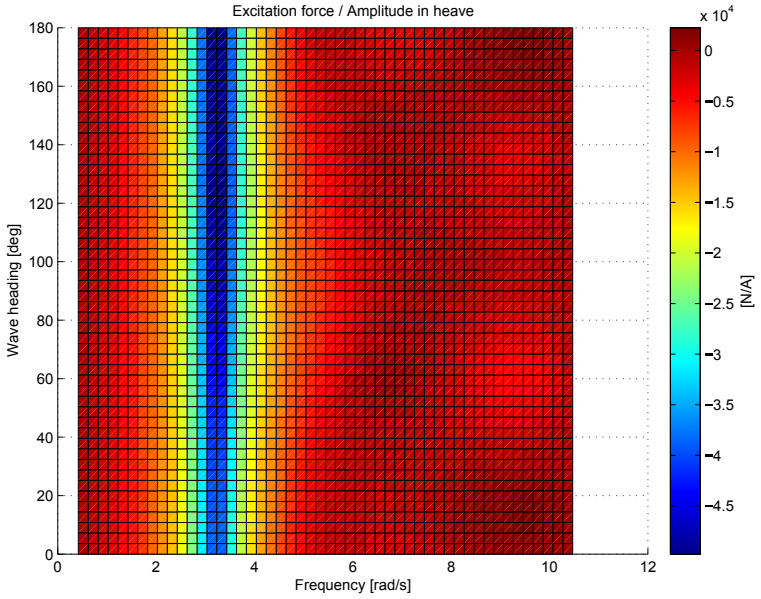

Figure A.15: Excitation load amplitude in heave for different headings and wave frequencies

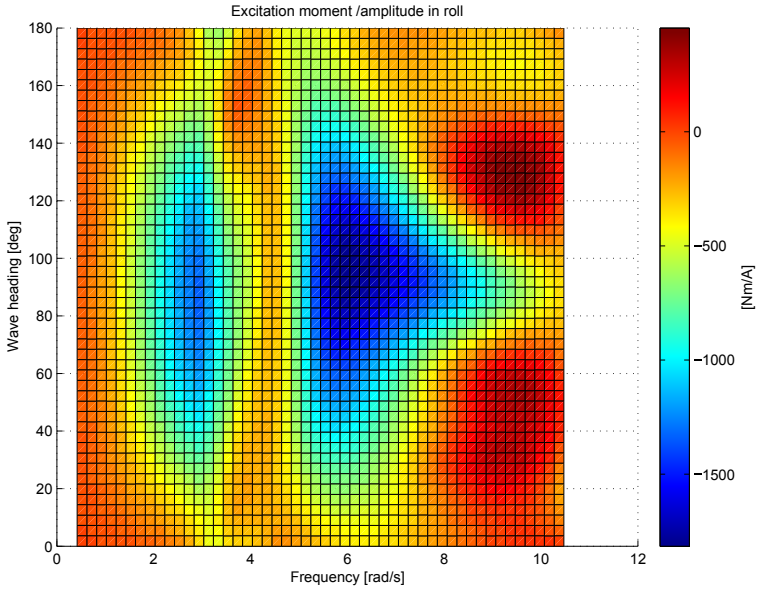

Figure A.16: Excitation load amplitude in roll for different headings and wave frequencies

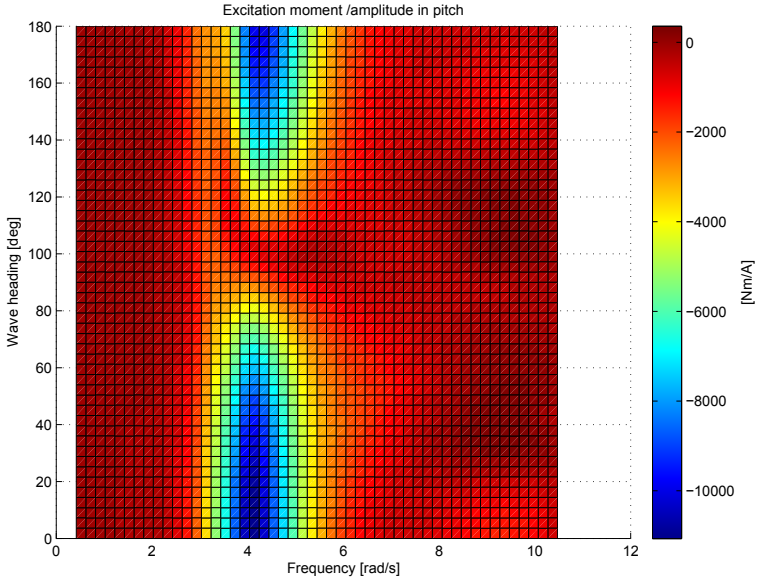

Figure A.17: Excitation load amplitude in pitch for different headings and wave frequencies

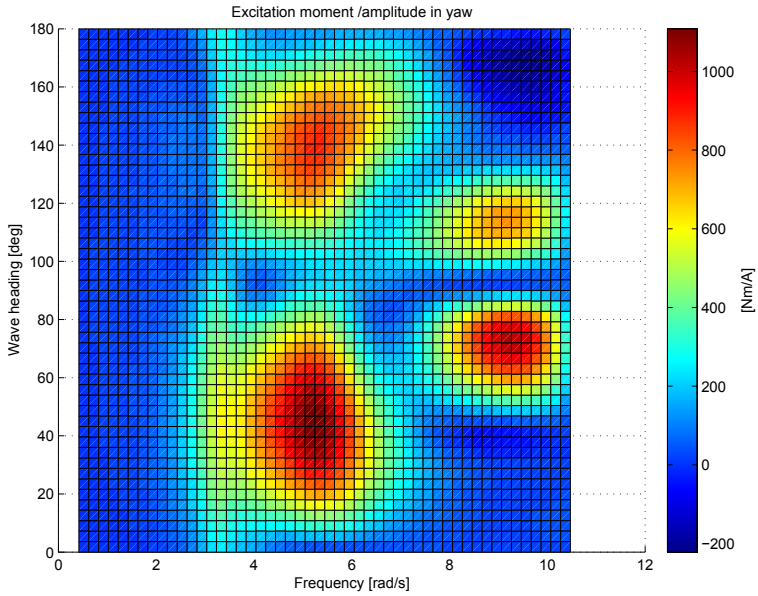

Figure A.18: Excitation load amplitude in yaw for different headings and wave frequencies

Appendix B

Fluid memory effect

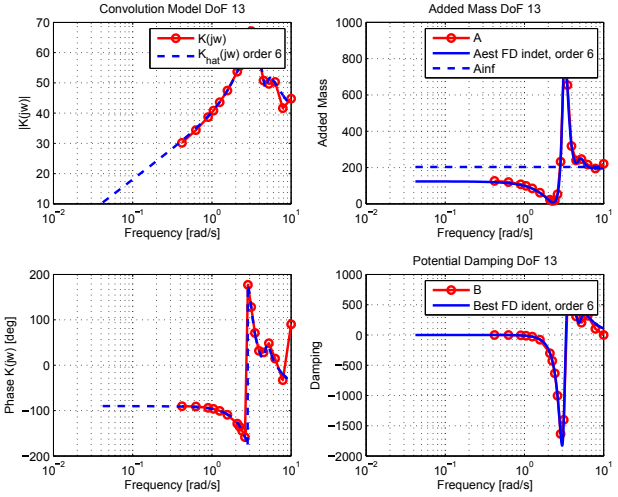

Figure B.1: ROV indentification results for $h_{13}(s)$. The left-hand side plots show the complex coefficients and its estimate while added mass and damping are plotted on the right-hand-side-plots

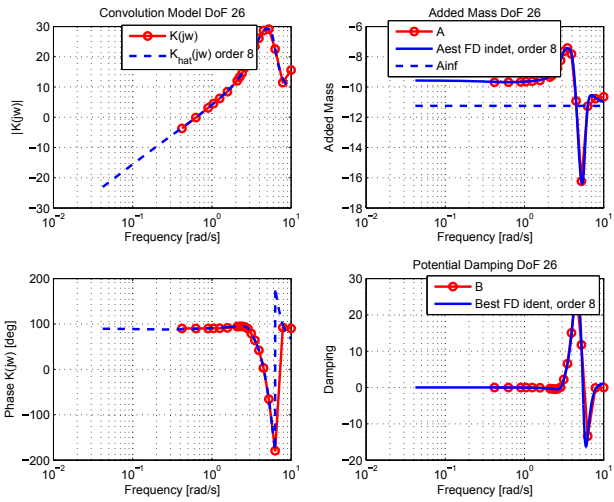

Figure B.2: ROV indentification results for $h_{26}(s)$. The left-hand side plots show the complex coefficients and its estimate while added mass and damping are plotted on the right-hand-side-plots